Table 3
The number of training sets and test sets

(A)

	Training	Test
Non HCC	43	11
HCC	41	13

(B)

	Training	Test
Well	16	8
Moderate	20	7

(C)

	Training	Test
AFP< 10(ng/ml)	20	4
AFP> 10(ng/ml)	14	10

(A) HCC, (B) histological grade, (C) AFP level.

a variable to class discrimination. Thus, we can eliminate irrelevant variables without any threshold. The R package used for stochastic gradient boosting, gbm, is available at http://cran.r-project.org.

3. Results and discussions

3.1. Proteomic profiling of non HCC and HCC tissues using 2D-DIGE

Labeled protein samples were separated on 2-DE, and fluorescence images were obtained. In parallel to the analytical gels, samples prepared from non HCC and HCC tissues were separately run on the preparative gels for protein identification. The proteins were visualized with SYPRO Ruby, and images were directly matched to CyDye images of analytical gels. Since 184 spots (125 proteins) consistently expressed in at least 70% of the all gels, we identified them as the proteins with consolidated expression intensities. Note that histological grade of moderate/well and high/low AFP level gels are derived from HCC samples only. Although we detected thousands spots on 2D gels, most of them are remained as unidentified. To enable us to interpret biologically, we analyzed identified spots only.

As mentioned in section 2.2, since the non HCC sample was labeled with Cy3 (or Cy5) dye, and the HCC sample was labeled with Cy5 (or Cy3) dye, we obtained three gels from one tissue sample. The numbers of HCC and non HCC gels, histological grade of moderate/well ones and high/low AFP ones are shown in Table 2.

3.2. Detection of proteins associated with HCC, histological grade and AFP level

To detect of the proteins associated with HCC, histological grade and AFP level, we performed supervised feature selection as described in section 2.10. To validate discriminative ability of selected spots, we randomly divided all gels to training sets and test sets. The number of training sets and test sets are summarized in Table 3. Since the number of HCC and non HCC gels was large, the rate of training sets and test sets was fixed about 4:1. On the other hand, since the number of images used to histological grade and AFP level was relatively small, the rate of training sets and test sets was set about 3:1 in cell differentiation and AFP level. We employed training sets for feature selection and constructing the predictive model. To detect spots associated with histological grade and AFP level, we used only HCC samples. The overall procedure is illustrated in Fig. 3. According to the previous study [21], we employed the parameters f, and M of SGB as 0.9, 0.01 and 1000, respectively. Table 4 show the selected spots associated with HCC, histological grade of moderate/well and AFP level. Other annotation data for these spots in Table S1 (Supplementary material). The number of selected spots associated with HCC, histological grade and AFP level is 18, 25 and 27, respectively. Although there are spots whose ratios are close to one, they are informative spots, because SGB is able to detect them as discriminative spots unlike statistical test for univariate, e.g., t-test. The positions of selected spots in the preparative 2D gel are shown in Fig. 4.

3.3. Evaluation of classification performance

We evaluated the classification performance by the selected spots on the basis of test sets according to the procedure illustrated in Fig. 3. This evaluation procedure is reasonable in terms of supervised prediction as discussed by Dupuy and Simon [27]. The performance was evaluated based on accuracy. Accuracy is defined as follows.

$$\text{accuracy} = \frac{\text{number of correctly predicted samples}}{\text{number of all samples}}$$

We constructed the predictive models using selected spots and training sets and applied to test sets as shown in Fig. 3. Table 5 shows the classification performance of SGB for HCC/non HCC, histological grade of moderate/well and high AFP (AFP> 10(ng/ml))/low AFP (AFP< 10(ng/ml)) level. From Table 5, SGB is able to classify both training sets

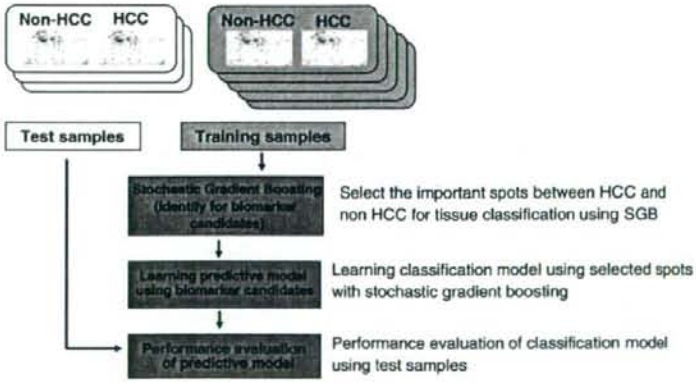

Fig. 3 Illustration of overall procedure for performance evaluation for HCC/non HCC classification. In histological grade of moderate/well grade and high/low AFP level, the same procedure is employed.

Table 4
Selected spots by SGB

(A) HCC

ID	SGB variable importance	Decyder		Protein name
		Ratio[a]	p-value (t-test)	
1977	30.66595	0.36	<1.0E−17	Carbonic anhydrase 2
560	29.66868	2.17	2.20E−13	Heat shock protein 90 kDa alpha
789	23.52533	1.84	2.20E−16	Annexin A6
1699	9.47421	6.98	<1.0E−17	Aldo-keto reductase family 1, member B10
366	3.07334	1.76	<1.0E−17	Heat shock 70 kDa protein 4
718	1.87712	2.12	5.70E−09	Heat shock 70 kDa protein 5
2012	0.71447	0.55	<1.0E−17	Enoyl Coenzyme A hydratase, short chain, 1
564	0.37075	1.37	0.0003	Transferrin
1007	0.15318	1.61	3.10E−07	Protein disulfide isomerase-associated 3
1556	0.12636	0.67	6.70E−10	Aldo-keto reductase 1A1
782	0.11134	1.7	1.40E−12	Heat shock 70 kDa protein 8
1331	0.05304	0.47	2.70E−13	Argininosuccinate synthetase
1312	0.05231	0.46	1.90E−09	Argininosuccinate synthetase
1046	0.05206	2.16	<1.0E−17	Vimentin
1582	0.04124	0.52	2.60E−11	Fructose-1,6-bisphosphatase 1
753	0.03851	1.79	3.60E−15	Heat shock 70 kDa protein 9B
2412	0.00211	0.54	3.00E−11	Human fatty acid binding protein FABP
444	0.00001	1.57	5.20E−06	Alpha glucosidase 2

(B) Histological grade

ID	SGB variable importance	Decyder		Protein name
		Ratio[b]	p-value (t-test)	
1129	49.9428	1.8	0.06	Keratin 8
1699	22.8444	0.43	2.00E−06	Aldo-keto reductase family 1, member B10
2423	5.616	1.38	0.064	D-dopachrome tautomerase
2126	4.7494	0.64	0.00041	peroxiredoxin 3
1068	4.6065	0.78	0.061	Glutamate dehydrogenase 1
2082	3.9313	0.77	0.0012	Es1 protein isoform 1a
1044	2.3596	0.61	0.068	Aldehyde dehydrogenase 1 family, member A1
999	1.6503	0.81	0.0033	Formiminotransferase cyclodeaminase
2039	1.2688	0.77	0.0088	Rho GDP dissociation inhibitor alpha
1685	1.1069	0.49	1.00E−05	Aldo-keto reductase 1B10
2025	0.6014	0.9	0.55	Heat shock 27 kDa protein 1
1036	0.4462	0.63	0.025	Aldehyde dehydrogenase 1 family, member A1
1059	0.3658	0.73	0.0054	Leucine aminopeptidase 3
1016	0.3094	0.98	0.11	Glucose regulated protein, 58 kDa
1027	0.0579	0.67	0.021	aldehyde dehydrogenase 1A1
1054	0.0558	0.73	0.015	Glutamate dehydrogenase 1
2159	0.0462	0.69	0.00038	Abhydrolase domain containing 14B
235	0.0204	1.13	0.48	Carbamoyl-phosphate synthetase 1
966	0.007	0.75	0.017	UDP-glucose dehydrogenase
2238	0.0044	0.93	0.054	Non-metastatic cells 1 protein
1086	0.003	0.98	0.87	UDP-glucose pyrophosphorylase 2
782	0.0025	1.19	0.25	Heat shock 70 kDa protein 8
2201	0.0018	0.76	0.025	Prostatic binding protein
1842	0.001	0.84	0.11	Electron-transfer-flavoprotein alpha subunit
798	0.0004	0.78	0.0021	Programmed cell death 8
1510	0.0004	0.78	0.0017	Acyl-Coenzyme A dehydrogenase, short/branched chain
1414	0.0001	0.93	0.14	Acetyl-Coenzyme A acetyltransferase 1

(C) AFP level

ID	SGB variable importance	Decyder		Protein name
		Ratio[c]	p-value (t-test)	
798	22.143	0.76	0.0002	Programmed cell death 8
1129	21.8696	1.62	0.25	Keratin 8
1007	12.4499	0.69	0.018	Protein disulfide isomerase-associated 3
1515	10.5222	0.81	0.95	Galactokinase 1
451	10.1806	0.85	0.37	Glucosidase, alpha; neutral AB
2159	7.1303	0.64	0.0065	Abhydrolase domain containing 14B
782	2.8347	1.18	0.0045	Annexin A6
659	2.7554	1.37	0.055	Lamin A/C
808	2.1413	0.7	0.0039	Carnitine palmitoyltransferase 2

Table 4 (continued)

(C) AFP level

ID	SGB variable importance	Decyder		Protein name
		Ratio[a]	p-value (t-test)	
1414	1.4418	0.81	0.01	Acetyl-Coenzyme A acetyltransferase 1
2082	1.4242	0.79	0.00028	Es1 protein isoform 1a
1219	1.2098	0.69	0.0083	Enolase 1
2010	1.1381	1.26	0.62	Enoyl-coenzyme A hydratase 1
1376	1.0921	0.61	0.00098	Actin, beta
2347	0.9536	1.35	0.001	Hemoglobin, beta
2364	0.2937	2.28	0.00013	Hemoglobin, beta
1794	0.1273	1.51	0.36	Sulfotransferase family, cytosolic, 2A, dehydroepiandrosterone-preferring, member 1
1383	0.0946	1.16	0.034	Aminoacylase 1
2423	0.0842	0.99	0.2	D-dopachrome tautomerase
1145	0.0647	0.95	0.058	ATP synthase, H+ transporting, mitochondrial F1 complex, beta polypeptide
1889	0.0281	1.12	0.41	Ketohexokinase
1795	0.0131	1.33	0.95	Sulfotransferase family, cytosolic, 2A, dehydroepiandrosterone (DHEA) -preferring, member 1
235	0.0045	0.87	0.063	Carbamoyl-phosphate synthetase 1, mitochondrial
1551	0.0028	1.35	0.7	Arginase 1
2039	0.0003	1.03	0.15	Rho GDP dissociation inhibitor alpha

[a] Ratio represents the average spot volume ratio of HCC/non HCC.
[b] Ratio represents the average spot volume ratio of moderate/well.
[c] Ratio represents the average spot volume ratio of high AFP/low AFP.

and test sets overall. For HCC and histological grade, SGB performs very well. For AFP, the accuracy of test sets is 71.4%. Although the performance of SGB depends on data sets, present results suggest that the spots selected by SGB are discriminative. From Table 4 (A)–(C), one can see that variable importance does not always correspond to p-value of t-test. This difference originates from that variable importance simultaneously incorporates multiple spots to classify the groups as described in Section 2.10, while t-test only incorporates average of each spots. Accordingly, one can detect the informative spots that contribute to sample classification through SGB. These discussions explain that SGB worked well for AFP in spite of the average spot value ratio of almost one.

To visualize the degree of discrimination for each data set by the selected spots, we show the scatter plots by two spots for each class in Fig. 5. One can see that the two spots discriminate each gel better than one spot. Thus, we demonstrated that supervised feature selection surely works well for detection of discriminative and informative proteins. Our results suggest that the SGB is able to detect the spots associated with tissue types using only identified spots.

3.4. Protein spots associated with HCC, histological grade and AFP

From Table 4(A), heat shock proteins (heat shock protein 90 kDa alpha, heat shock 70 kDa protein 4, heat shock 70 kDa protein 5, heat shock 70 kDa protein 8, heat shock 70 kDa protein 9B), protein disulfide isomerase-associated 3 (PDIA3) and aldo-keto reductase 1B10 (AKRB10) were overexpressed in HCC. These events are common at least three members of HSP family (HSP90, HSP70, HSC71) have been reported in prior works [14,28,29]. Members of the heat shock protein family have been known to promote cancer cell growth and survival by distinct mechanism [30]. HSP family were first discovered by their elevated abundance after heat shock. They take part in protein folding processes in normal physiological conditions. They bind and prevent non-native proteins from aggregation. Heat shock 70 kDa protein 5 (GRP78) is a member of HSP70 family localized in endoplasmic reticulum (ER). Expression of GRP78 can be induced in response to different stimuli including glucose starvation, hypoxia and ER

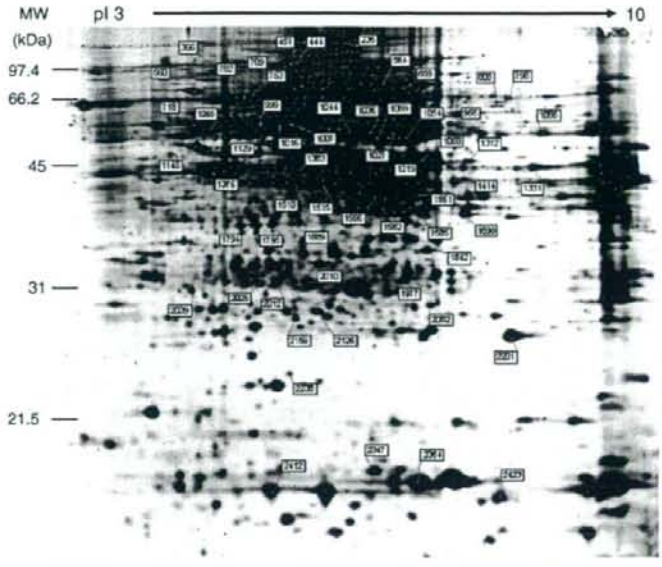

Fig. 4. Representative 2D image of the preparative gel. The gel was post-stained with SYPRO Ruby (Invitrogen). The numbers indicate spots associated with HCC, spots associated with grade and spots associated with AFP.

Ca2+ pool depletion [31]. GRP78 has been proven to protect cells from apoptosis, probably through inhibition of caspase-7 activation, an apoptotic executioner [32]. Highly induced GRP78 in progressively growing tumor cells has been reported to protect them from immune attack, thus preventing tumor regression [33]. High level of GRP78 observed in this study may also support the aggressive growth and the suppression of tumor rejection in HCC. In this study, carbonic anhydrase 2 (CAII) is poorly expressed in HCC, being consistent with the report of Kuo et al. [34] They concluded that this might promote tumor cell motility and contribute to tumor growth and metastasis.

In addition, heat shock 70 kDa protein 9B (mortalin) is abundantly expressed in HCC. Yi et al. [35] recently found that overexpression of mortalin in HCC was associated with HCC metastasis and early recurrence using 2-DE, quantitative PCR, western blot and immunohistochemistry. Poor expression of argininosuccinate synthetase (ASS) is one of well-known molecular features of HCC and is recently a target of HCC treatment using arginine-depleting enzymes [36]. Vimentin (VIM) is abundantly expressed in HCC. Hu et al. [37] reported that overexpression of VIM is significantly associated with HCC metastasis using cDNA microarray and tissue microarray.

Table 5
Performance evaluation for classification

Training sets	
Data sets	Accuracy (%)
HCC/non HCC	100
Moderate/well	100
Low AFP/high AFP	94.1
Test sets	
Data sets	Accuracy (%)
HCC/non HCC	100
Moderate/well	93.3
Low AFP/high AFP	71.4

(a) HCC (HCC/non HCC), (b) histological grade (moderate/well), (c) AFP level (low AFP/high AFP).

Furthermore, we examined gene expression level of selected proteins by RTD-PCR and cDNA microarray (Table S1 (a)). Most of these results are also consistent with protein expression profiles.

Although previous studies dealt with large size HCC or HCC with progressive stage, we dealt with small size HCC in this study. The proteins shown here might be potential biomarkers for early diagnosis.

Table 4 (B) and (C) represent protein spots associated with histological grade in HCC, and protein spots associated with AFP level, respectively. Table 4 (B) shows that several metabolic enzymes, such as AKRB10, glutamate dehydrogenase 1 (GLUD1), aldehyde dehydrogenase 1A1, and peroxiredoxin3 (PRDX3) were poorly expressed in moderate HCC cells, and keratin 8 (KRT8) were abundantly expressed in moderate HCC. It has been reported that the message of AKR1B10 was expressed most abundantly in small intestine and colon, while with lower levels in liver, thymus, prostate, testis, and skeletal muscle in normal tissues [38]. From our results, although AKR1B10 abundantly expressed in HCC compared with non HCC, it poorly expressed in moderate grade compared with well grade. The reason of this could be explained well, however different metabolic process in moderate differentiated HCC might not support the high expression of this gene as found in well differentiated HCC. GLUD1 has been reported poorly expressed in HCC [39]. This may suggest that GLUD1 is related to both HCC and grade. PRDX3 is required for MYC-mediated proliferation, transformation, and apoptosis after glucose withdrawal and essential for maintaining mitochondrial mass and membrane potential in transformed rat and human cells and deregulated expression of the MYC transcription factor is found in a wide variety of human tumors. These data provided evidence that PRDX3 is a MYC target gene that is required to maintain normal mitochondrial function [40].

AFP is the most established tumor marker in HCC and the gold standard by which other markers for the disease are judged [41]. Approximately, 70% of HCC are associated with AFP, and some HCC produce low level of AFP. Although small tumors tend to produce lower levels of AFP, direct relationship between serum AFP and tumor size has not been established as yet. Younger patients and men tend to have higher levels compared to older patients and women, respectively

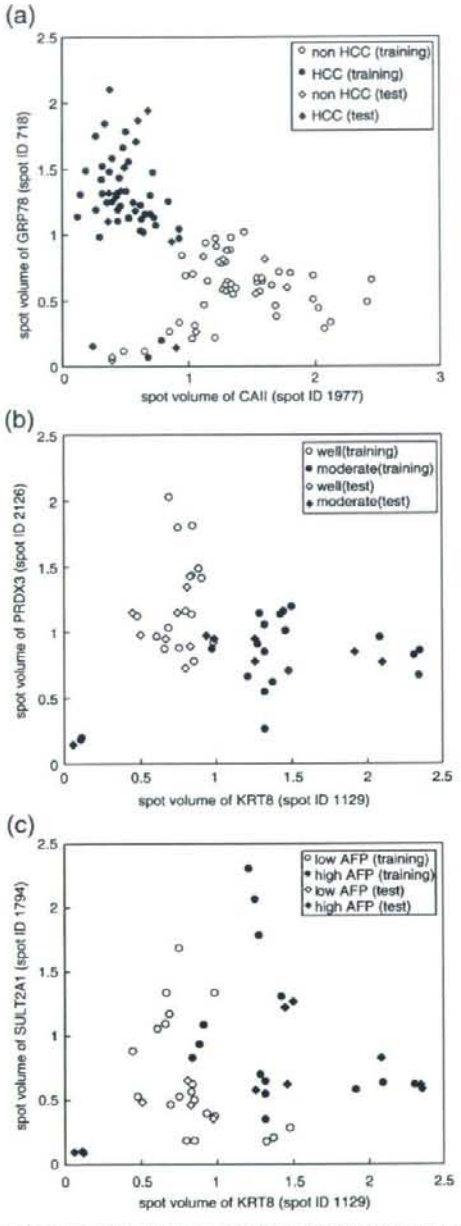

Fig. 5. The scatter plots by two spots. (a) HCC/non HCC, (b) histological grade of moderate/well, (c) high AFP/low AFP level.

[42,43]. From Table 4 (C), two structural protein, KRT8 and lamin A/C were abundantly expressed in HCC cells associated with higher levels of AFP, whereas two apotosis related proteins, programmed cell death 8 and sulfotransferase family, cytosolic, 2A, dehydroepiandrosterone-prefering, member1 (SULT2A1) and PDIA3 were poorly expressed in HCC cells associated with higher levels of AFP.

The overexpression of KRT8 also has been reported by Western blot and immunofluorescence analysis in higher metastatic HCC cell lines [44]. This implies that the alternation of KRT8 in its expression level might be related to metastatic ability. In this study, we observed that KRT8 expressed abundantly in both moderate HCC and high AFP level.

Chignard et al. has reported that a highly significant difference in PDIA3 fragment serum levels among HCC patients, at-risk patients (patients with chronic hepatitis or cirrhosis) and healthy individuals was observed [45]. However, they did not investigate the correlation between HCC and AFP. On the other hand, we observed that PDIA3 was poorly expressed in HCC cells associated with higher levels of AFP. Hence, our results suggest that AFP and PDIA3 may be complementarily expressed abundantly in serum.

Note that the differentially expressed proteins associated with histological grade of HCC and AFP level found in this study, are not always specific for HCC. PDIA3 has been reported to be differentially expressed in brain and breast cancer [46,47]. AKR1B10 has been involved also in lung cancer [48]. Also, it has been known that cytokeratins including KRT8 are part of the epithelial–mesenchymal transition (EMT). EMT is originally an embryonic developmental process that is hijacked by cancer cells in colorectal cancer [49]. However, our finding in this pilot study could provide new insights on understanding the pathogenesis of HCC, histological grade and AFP level.

4. Conclusion

We performed 2D-DIGE combined with MS to analyze the proteomic profiling of HCC and their surrounding non HCC obtained from 18 HCC patients. We identified the discriminative and informative protein spots associated with HCC, histological grade and AFP level using feature selection with SGB. We confirmed that the proposed method is able to identify known HCC-related proteins, e.g., HSP70 family. Moreover, we identified the potential biomarkers associated with histological grade of HCC and AFP level and found that AKR1B10 is related to,well differentiated HCC KRT8 is related to both cell differentiation and AFP level and PDIA3 is associated with both HCC and AFP level. Although the list of selected spots can be changed depending on training sets as pointed by Michiels et .al. [50], we showed that our present results for HCC are consistent with many prior studies and it appears that the obtained results are certainly reliable. Since all HCC samples were stage I, we observed the molecular events of relatively early stage of tumor. Our results shed light on understanding of the pathogenesis mechanism of HCC, histological grade and AFP level and will contribute to therapy and treatments for HCC. Although we only deal with small number of samples in this study, our strategy may be useful for detection of diagnosis or prognosis biomarkers when large number of samples are available.

Acknowledgement

The authors thank to Naoko Tetsura for excellent technical assistance.

Appendix A. Supplementary data

Supplementary data associated with this article can be found, in the online version, at doi:10.1016/j.bbapap.2008.02.011.

References

[1] D.M. Parkin, P. Pisani, J. Ferlay, Global cancer statistics, Cancer J. Clin. 49 (1999) 33–64.
[2] P. Pisani, D.M. Parkin, F. Bray, J. Ferley, Estimates of the world wide mortality from 25 cancers in 1990, Int. J. Cancer 83 (1999) 18–29.
[3] H.B. El-Serag, A.C. Mason, Rising incidence of hepatocelluar carcinoma in the United States, N. Engl. J. Med. 340 (1999) 745–750.

[4] S.D. Taylor-Robinson, G.R. Foster, S. Arora, H.C. Thomas, Increase in primary liver cancer in the UK, Lancet 350 (1997) 1142–1143.
[5] L.J. Lopez, J.A. Marrero, Hepatocellular carcinoma, Curr. Opin. Gastroenterol. 3 (2004) 248–253.
[6] H. Okabe, T. Satoh, T. Kato, O. Kitahara, R. Yanagawa, Y. Yamaoka, T. Tsunoda, Y. Furukawa, Y. Nakamura, Genomewide analysis of gene expression in human hepatocellular carcinomas using cDNA microarray: identification of genes involved in viral carcinogenesis and tumor progression, Cancer Res. 13 (2001) 2129–2137.
[7] X. Chen, S.T. Cheung, S. So, S.T. Fan, C. Barray, J. Higgins, K.M. Lai, J. Ji, S. Dudoit, I.O. Ng, M. Van De Rijn, D. Botstein, P.O. Brown, Gene expression patterns in human liver cancers, Mol. Biol. Cell 13 (2002) 1929–1939.
[8] M.W. Smith, Z.N. Yue, G.K. Geiss, N.Y. Sadovnikova, V.S. Carter, L. Boix, C.A. Lazaro, G.B. Rosenberg, R.E. Bumgarner, N. Fausto, J. Bruix, M.G. Katze, Identification of novel tumor markers in hepatitis C virus-associated hepatocellular carcinoma, Cancer Res. 63 (2003) 859–864.
[9] T. Yamashita, S. Kaneko, T. Hashimoto, S. Sato, N. Nagai, T. Toyoda, K. Suzuki, K. Kobayashi, K. Matsushima, Serial analysis of gene expression in chronic hepatitis C and hepatocellular carcinoma, Biochem. Biophys. Res. Commun. 282 (2001) 647–654.
[10] Q.H. Ye, L.X. Qin, M. Forgues, P. He, J.W. Kim, A.C. Peng, R. Simon, Y. Li, A.I. Robles, Y. Chen, Z.C. Ma, Z.Q. Wu, S. Ye, Y.K. Liu, Z.Y. Tang, X.W. Wang, Predicting hepatitis B virus-positive metastatic hepatocellular carcinoma using gene expression profiling and supervised machine learning, Nat. Med. 9 (2003) 416–423.
[11] P.J. Wirth, T.N. Hoang, T. Benjamin, Micorpreparative immobilized pH gradient two-dimensional electrophoresis in combination with protein microsequencing for the analysis of human liver proteins, Electrophoresis 16 (1995) 1946–1960.
[12] T.K. Seow, S.E. Ong, R.C. Liang, E.C. Ren, L. Chan, K. Ou, M.C. Chung, Two-dimensional electrophoresis map of the human hepatocellular carcinoma cell line, HCC-M, and identification of the separated proteins by mass spectrometry, Electrophoresis 21 (2000) 1787–1813.
[13] K.S. Park, S.Y. Cho, H. Kim, Y.K. Paik, Proteomic alternations of the variants of human aldehyde dehydrogenase isozymes correlate with hepatocellular carcinoma, Int. J. Cancer 97 (2002) 261–265.
[14] S.O. Lim, S.J. Park, W. Kim, S.G. Park, H.J. Kim, Y.I. Kim, T.S. Sohn, J.H. Noh, G. Jung, Proteomic analysis of hepatocellular carcinoma, Biochem. Biophys. Res. Commun. 291 (2002) 1031–1037.
[15] K.S. Park, H. Kim, N.G. Kim, S.Y. Cho, K.H. Choi, J.K. Seong, Y.K. Paik, Proteomic analysis and molecular characterization of tissue ferritin light chain in hepatocellular carcinoma, Hepatology 35 (2002) 1459–1466.
[16] M. Unlu, J.S. Morgan, J.S. Minden, Difference gel electrophoresis: a single gel method for detecting changes in protein extracts, Electrophoresis 11 (1997) 2071–2077.
[17] M.R. Knowles, S. Cervino, H.A. Skynner, S.P. Hunt, C. de Felipe, K. Salim, G. Meneses-Lorente, G. McAllister, P.C. Guest, Multiplex proteomic analysis by two-dimensional differential in gel electrophoresis, Proteomics 3 (2003) 1162–1171.
[18] J. Shaw, R. Rowlinson, J. Nickson, T. Stone, A. Sweet, K. Williams, R. Tonge, Evaluation of saturation labeling two-dimensional difference gel electrophoresis fluorescent dyes, Proteomics 3 (2003) 1181–1195.
[19] G. Van den Bergh, L. Arckens, Fluorescent two-dimensional difference gel electrophoresis unveils the potential of gel-based proteomics, Curr. Opin. Biotechnol. 15 (2004) 38–43.
[20] A. Alban, S.O. David, L. Bjorkesten, C. Anderson, E. Sloge, S. Lewis, I. Currie, A novel experimental design for comparative two-dimensional gel analysis: two-dimensional difference gel electrophoresis incorporating a pooled internal standard, Proteomics 1 (2003) 36–44.
[21] J.H. Friedman, Stochastic gradient boosting, Comput. Stat. Data Anal. 38 (2002) 367–378.
[22] K.G. Ishak, P.P. Anthony, L.H. Sobin, Histological typing Classification of Tumors, Springer-Verlag, New York, 1994.
[23] Minagawa, J., Honda, M., Miyazaki, K., Tabuse, Y., Teramoto, R., Yamashita, T., Nishino, K., Takatori, H., Ueda, T., Kamijo, K., Kaneko, S., Comparative proteomic and transcriptomic profiling of the human hepatocellular carcinoma. Biochem. Biophys. Res. Commun. in press.
[24] M. Honda, T. Yamashita, T. Ueda, R. Takatori, R. Nishino, S. Kaneko, Different signaling pathways in the livers of patients with chronic hepatitis B or chronic hepatitis C, Hepatology 44 (2006) 1122–1138.
[25] O. Troyanskaya, M. Cantor, G. Sherlock, P. Brown, T. Hastei, R. Tibshirani, D. Botstein, R.B. Altman, Missing value estimation methods for DNA microarrays, Bioinformatics 17 (2001) 520–525.
[26] J.H. Friedman, Greedy function approximation: a gradient boosting machine, Ann. Stat. 29 (2001) 1189–1232.
[27] A. Dupuy, R.M. Simon, Critical review of published microarray studies for cancer outcome and guidelines on statistical analysis and reporting, J. Natl. Cancer Inst. 99 (2007) 147–157 (99).
[28] M. Takashima, Y. Kuramitsu, Y. Yokoyama, N. Iizuka, T. Toda, I. Sakaida, K. Okita, M. Oka, K. Nakamura, Proteomic profiling of heat shock protein 70 family members as biomarkers for hepatitis C virus-related hepatocellular carcinoma, Proteomics 3 (2003) 2487–2493.
[29] W. Kim, S. Oe Lim, J.S. Kim, Y.H. Ryu, J.Y. Byeon, H.J. Kim, Y.I. Kim, J.S. Heo, Y.M. Park, G. Jung, Comparison of proteome between hepatitis B virus- and hepatitis C virus-associated hepatocelluar carcinoma, Clin. Cancer Res. 9 (2003) 5493–5500.
[30] M. Rohde, M. Daugaard, M.H. Jensen, K. Helin, J. Nylandsted, M. Jäättelä, Members of the heat-shock protein 70 family promote cancer cell growth by distinct mechanisms, Genes Dev. 19 (2005) 570–582.
[31] H. Miyake, I. Hara, S. Arakawa, S. Kamidono, Stress protein GRP78 prevents apoptosis induced by calcium ionophore, ionomycin, but not by glycosylation inhibitor, tunicamycin, in human prostate cancer cells, J. Cell. Biochem. 77 (2000) 396–408.
[32] R.K. Reddy, C. Mao, P. Baumeister, R.C. Austin, Endoplasmic reticulum chaperone protein GRP78 protects cells from apoptosis induced by topoisomerase inhibitors: role of ATP binding site in suppression of caspase-7 activation, J. Biol. Chem. 278 (2003) 20915–20924.
[33] C. Jamora, G. Dennert, A.S. Lee, Inhibition of tumor progression by suppression of stress protein GRP78/BiP induction in fibrosarcoma B/C10ME, Proc. Natl. Acad. Sci. U. S. A. 93 (1996) 7690–7694.
[34] W.H. Kuo, W.L. Chiang, S.F. Yang, K.T. Yeh, C.M. Yeh, Y.S. Hsieh, S.C. Chu, The differential expression of cytosolic carbonic anhydrase in human hepatocellular carcinoma, Life Sci. 73 (2003) 2211–2223.
[35] Yi, X., Luk, M. J., Lee, P. N., Peng, J., Leng, X., Guan, X., Lau, K. G., Fan, S., Association of mortalin (HSPA9) with liver cancer metastasis and prediction for early tumor recurrence. Mol. Cell. Proteomics. in press.
[36] N.P. Cheng, T. Lam, W. Lam, S. Tsui, W.A. Cheng, W. Lo, Y. Leung, Pegylated recombinant human arginase (rhArg-peg500mw) inhibits the in vitro and in vivo proliferation of human hepatocellular carcinoma through depletion, Cancer Res. 67 (2007) 309–317.
[37] L. Hu, H.S. Lau, C. Tzang, J. Wen, W. Wang, D. Xie, M. Huang, Y. Wang, M. Wu, J. Huang, W. Zeng, J. Sham, M. Yang, X. Guan, Association of vimentin overexpression and hepatocellular carcinoma metastasis, Oncogene 23 (2004) 298–302.
[38] D. Cao, S.T. Fans, S.S.M. Chung, Identification and characterization of a novel human aldose reductase-like gene, J. Biol. Chem. 273 (1998) 11429–11435.
[39] I.N. Lee, C.H. Chen, J.C. Sheu, H.S. Lee, G.T. Huang, C.Y. Yu, F.J. Lu, L.P. Chow, Identification of human hepatocellular carcinoma-related biomarkers by two-dimensional difference gel electrophoresis and mass spectrometry, J. Proteome Res. 4 (2005) 2062–2069.
[40] D.R. Wonsey, K.I. Zeller, C.V. Dang, The c-Myc target gene PRDX3 is required for mitochondrial homeostasis and neoplastic transformation, Proc. Natl. Acad. Sci. U. S. A. 99 (2002) 6649–6654.
[41] J.B. Lopez, Recent developments in the first detection of hepatocellular carcinoma, Clin. Biochem. Rev. 26 (2005) 65–79.
[42] M.C. Kew, Hepatocellular cancer: a century of progress, Clin. Liver Dis. 4 (2000) 257–268.
[43] P.J. Johnson, The role of serum alpha-fetoprotein estimation in the diagnosis and management of hepatocellular carcinoma, Clin. Liver Dis. 5 (2001) 145–160.
[44] Z. Dai, Y.K. Liu, J.F. Cui, H.L. Shen, J. Chen, R.X. Sun, Y. Zhang, X.W. Zhou, P.Y. Yang, Z.Y. Tang, Identification and analysis of altered alpha1,6-fucosylated glycoproteins associated with hepatocellular carcinoma metastasis, Proteomics 6 (2006) 5857–5867.
[45] N. Chignard, S. Shang, H. Wang, J. Marrero, C. Bréchot, S. Hanash, L. Bereretta, Cleavage of endoplasmic reticulum proteins in hepatocellular carcinoma: detection of generated fragments in patient sera, Gastroenterology 130 (2006) 2010–2022.
[46] F. Odreman, M. Vindigni, M.L. Gonzales, B. Niccolini, G. Candiano, B. Zanotti, M. Skrap, S. Pizzolitto, G. Stanta, A. Vindigni, Proteomic studies on low- and high-grade human brain astrocytomas, J. Proteome Res. 4 (2005) 698–708.
[47] K. Gumireddy, F. Sun, A.J. Klein-Szanto, J.M. Gibbins, P.A. Gimotty, A.J. Saunders, P.G. Schultz, Q. Huang, In vivo selection for metastasis promoting genes in the mouse, Proc. Natl. Acad. Sci. U. S. A. 16 (2007) 6696–6701.
[48] S. Fukumoto, N. Yamauchi, H. Moriguchi, Y. Hippo, A. Watanabe, J. Shibahara, H. Taniguchi, S. Ishikawa, H. Ito, S. Yamamoto, H. Iwanari, M. Hironaka, Y. Ishikawa, T. Niki, Y. Sohara, T. Kodama, M. Nishimura, M. Fukayama, H. Dosaka-Akita, H. Aburatani, Overexpression of the aldo-keto reductase family protein AKR1B10 is highly correlated with smokers' non-small cell lung carcinomas, Clin. Cancer Res. 5 (2005) 1776–1785.
[49] T. Knösel, V. Emde, K. Schlüns, P.M. Schlag, M. Dietel, I. Petersen, Cytokeratin profiles identify diagnostic signatures in colorectal cancer using multiplex analysis of tissue microarrays, Cell. Oncol. 28 (2006) 167–175.
[50] S. Michiels, S. Koscielny, C. Hill, Prediction of cancer outcome with microarrays: a multiple random validation strategy, Lancet 365 (2005) 488–492.

Available online at www.sciencedirect.com
ScienceDirect
Biochemical and Biophysical Research Communications 366 (2008) 186–192
BBRC
www.elsevier.com/locate/ybbrc

Comparative proteomic and transcriptomic profiling of the human hepatocellular carcinoma

Hirotaka Minagawa [a], Masao Honda [b,*], Kenji Miyazaki [c], Yo Tabuse [c,*], Reiji Teramoto [c], Taro Yamashita [b], Ryuhei Nishino [b], Hajime Takatori [b], Teruyuki Ueda [b], Ken'ichi Kamijo [a], Shuichi Kaneko [b]

[a] *Nano Electronics Research Laboratories, NEC Corporation, 34, Miyukigaoka, Tsukuba, Ibaraki 305-8501, Japan*
[b] *Department of Gastroenterology, Kanazawa University Graduate School of Medical Science, Kanazawa, 13-1 Takara-machi, Kanazawa 920-8641, Japan*
[c] *Bio-IT Center, NEC Corporation, 34, Miyukigaoka, Tsukuba, Ibaraki 305-8501, Japan*

Received 14 November 2007
Available online 4 December 2007

Abstract

Proteome analysis of human hepatocellular carcinoma (HCC) was done using two-dimensional difference gel electrophoresis. To gain an understanding of the molecular events accompanying HCC development, we compared the protein expression profiles of HCC and non-HCC tissue from 14 patients to the mRNA expression profiles of the same samples made from a cDNA microarray. A total of 125 proteins were identified, and the expression profiles of 93 proteins (149 spots) were compared to the mRNA expression profiles. The overall protein expression ratios correlated well with the mRNA ratios between HCC and non-HCC (Pearson's correlation coefficient: $r = 0.73$). Particularly, the HCC/non-HCC expression ratios of proteins involved in metabolic processes showed significant correlation to those of mRNA ($r = 0.9$). A considerable number of proteins were expressed as multiple spots. Among them, several proteins showed spot-to-spot differences in expression level and their expression ratios between HCC and non-HCC poorly correlated to mRNA ratios. Such multi-spotted proteins might arise as a consequence of post-translational modifications.

Keywords: Hepatocellular carcinoma; Proteome; Two-dimensional difference gel electrophoresis; Transcriptome; cDNA microarray

Hepatocellular carcinoma (HCC) is one of the most common cancers worldwide, and a leading cause of death in Africa and Asia [1]. Although several major risks related to HCC, such as hepatitis B and/or hepatitis C virus infection, aflatoxin B1 exposure, and alcohol consumption, and genetic defects, have been revealed [2], the molecular mechanisms leading to the initiation and progression of HCC are not well known. To find the molecular basis of hepatocarcinogenesis, comprehensive gene expression analyses have been done using many systems such as hepatoma cell lines and tissue samples [3,4]. Previously, we have carried out a comprehensive mRNA expression analysis using the serial analysis of gene expression (SAGE) [5] and cDNA microarray-based comparative genomic hybridization [6] to acquire the outline of gene expression profile of HCC. Although these genomic approaches have yielded global gene expression profiles in HCC and identified a number of candidate genes as biomarkers useful for cancer staging, prediction of prognosis, and treatment selection [7], the molecular events accompanying HCC development are not yet understood. In general, proteins rather than transcripts are the major effectors of cellular and tissue function [8] and it is accepted that protein expression do not always correlate with mRNA expression [9,10]. Thus, protein expression analysis, which could complement the available mRNA data, is also important to understand the molecular mechanisms of HCC.

* Corresponding authors. Fax: +81 76 234 4250 (M. Honda), +81 29 856 6136 (Y.Tabuse).
E-mail addresses: mhonda@medf.m.kanazawa-u.ac.jp (M. Honda), y-tabuse@cd.jp.nec.com (Y. Tabuse).

0006-291X/$ - see front matter © 2007 Elsevier Inc. All rights reserved.
doi:10.1016/j.bbrc.2007.11.101

The technique of two-dimensional difference gel electrophoresis (2D-DIGE), developed by Unlu et al. [11] is one of major advances in quantitative proteomics. Several groups have recently utilized 2D-DIGE to examine protein expression changes in HCC samples [12,13], whereas reports on the analysis combining both transcriptomic and proteomic approach are rare.

In the present study, we compared quantitatively protein expression profiles of HCC to non-HCC (non-cancerous liver) samples derived from 14 patients by 2D-DIGE. We also compared the protein expression profiles of the same HCC and non-HCC samples to the mRNA profiles which have been obtained using a cDNA microarray. The expression ratios of 93 proteins showed significant correlations with the mRNA ratios between HCC and non-HCC. Proteins involved in metabolic processes showed more prominent correlation. Our study describes an outline of gene and protein expression profiles in HCC, thus providing us a basis for better understanding of the disease.

Materials and methods

Patients. A total of 14 HCC patients who had surgical resection done in the Kanazawa University Hospital were enrolled. The clinicopathological characteristics of them are shown in Table 1. The HCC samples and adjacent non-tumor liver samples were snap frozen in liquid nitrogen, and used for cDNA microarray and 2D-DIGE analysis. All HCC and non-tumor samples were histologically diagnosed and quantitative detection of hepatitis C virus RNA by Amplicore analysis (Roche Diagnostic Systems) showed positive. The grading and staging of chronic hepatitis associated with non-tumor lesion were histologically assessed according to the method described by Desmet et al. [14] and histological typing of HCC was assessed according to Ishak et al. [15]. All strategies used for gene expression and protein expression analysis were approved by the Ethical Committee of Kanazawa University Hospital.

Preparation of cDNA microarray slides. In addition to in-house cDNA microarray slides consisting of 1080 cDNA clones as previously described [6,16–18], we made new cDNA microarray slides for detailed analysis of the signaling pathway of metabolism and enzyme function in liver disease [19]. Besides cDNA microarray analysis, a total of 256,550 tags were obtained from hepatic SAGE libraries (derived from normal liver, CH-C, CH-C related HCC, CH-B, and CH-B related HCC), including 52,149 unique tags. Among these, 16,916 tags expressing more than two hits were selected to avoid the effect of sequencing errors in the libraries. From these candidate genes, 9614 non-redundant clones were obtained from Incyte Genomics (Incyte Corporation), Clontech (Nippon Becton Dickinson), and Invitrogen (Invitrogen). Each clone was sequence validated and PCR amplified by Dragon Genomics (Takara Bio), and the cDNA microarray slides (Liver chip 10k) were constructed using SPBIO 2000 (Hitachi Software) as described previously [6,16–18].

Table 1
Characteristics of patients involved in this study

Patient No.	Age	Sex[a]	Histology of non-tumor lesion[b]	Tumor histology	Viral status
1	64	M	F4A1	Moderate	HCV
2	65	M	F4A1	Well	HCV
3	48	M	F3A1	Moderate	HCV
4	69	F	F4A2	Moderate	HCV
5	66	F	F4A2	Well	HCV
6	45	M	F4A1	Well	HCV
7	75	F	F4A1	Well	HCV
8	46	M	F4A2	Moderate	HCV
9	66	M	F2A2	Well	HCV
10	75	M	F3A1	Moderate	HCV
11	67	F	F4A2	Well	HCV
12	64	M	F4A1	Moderate	HCV
13	68	M	F4A0	Well	HCV
14	74	M	F1A0	Moderate	HCV

[a] M, male; F, female.
[b] F, fibrosis; A, activity.

RNA isolation and antisense RNA amplification. Total RNA was isolated from liver biopsy samples using an RNA extraction kit (Stratagene). Aliquots of total RNA (5 μg) were subjected to amplification with antisense RNA (aRNA) using a Message AmpTM aRNA kit (Ambion) as recommended by the manufacturer. About 25 μg of aRNA was amplified from 5 μg total RNA, assuming that 500-fold amplification of mRNA was obtained. The quality and degradation of the isolated RNA were estimated after electrophoresis using an Agilent 2001 bioanalyzer. In addition, 10 μg of aRNA was used for further labeling procedures.

Hybridization on cDNA microarray slides and image analysis. As a reference for each microarray analysis, aRNA samples prepared from the normal liver tissue from one of the patients were used. Test RNA samples fluorescently labeled with cyanine (Cy) 5 and reference RNA labeled with Cy3 were used for microarray hybridization as described previously [6,16–18]. Quantitative assessment of the signals on the slides was done by scanning on a ScanArray 5000 (General Scanning) followed by image analysis using GenePix Pro 4.1 (Axon Instruments) as described previously [6,16–18].

Protein expression analysis using 2D-DIGE. Protein samples were homogenized with lysis buffer (7 M urea, 2 M thiourea, 4% w/v CHAPS, 0.8 μM aprotinin, 15 μM pepstatin, 0.1 mM PMSF, 0.5 mM EDTA, 30 mM Tris–HCl, pH 8.5) and centrifuged at 13,000 rpm for 20 min at 4 °C. The supernatants were used as protein samples. The protein concentrations were determined with a protein assay reagent (Bio-Rad). The non-HCC and HCC samples (50 μg each) labeled with either Cy3 or Cy5 according to the manufacture's manual were combined and separated on 2-DE gels together with the Cy2-labeled internal standard (IS), which was prepared by mixing equal amounts of all samples. Analytical 2-DE was performed as described previously [20] using Immobiline DryStrip (pH 3–10, 24 cm, GE Healthcare) in the first dimension and 12.5% SDS–polyacrylamide gels (24 × 20 cm) in the second dimension. Samples were run in triplicate to obtain statistically reasonable results. After scanning with a Typhoon 9410 scanner (GE Healthcare), gels were silver stained for protein identification. For protein identification, 400 μg of the IS sample was also separately run on a 2-DE gel and stained with SYPRO Ruby (Invitrogen). All analytical and preparative gel images were processed using ImageQuant (GE Healthcare) and the protein level analysis was done with the DeCyder software (GE Healthcare). To detect phosphoproteins, 400 μg of HCC and non-HCC samples were separately run on 2-DE gels and stained with ProQ Diamond (Invitrogen). After acquiring images, gels were counterstained with SYPRO Ruby to visualize total proteins as described above.

Protein identification. The excised protein spots were in-gel digested with porcine trypsin (Promega). For LC-ESI-IT MS/MS analysis using LCQ Deca XP (Thermo Electron), the digested and dried peptides were dissolved in 10 μl of 0.1% formic acid in 2% acetonitrile (ACN). The dissolved samples were loaded onto C18 silica gel capillary columns (Magic C18, 50 × 0.2 mm), and the elution from the column was directly connected through a sprayer to an ESI-IT MS. Mobile phase A was 2% ACN containing 0.1% formic acid, and mobile phase B was 90% ACN containing 0.1% formic acid. A linear gradient from 5% to 65% of concentration B was applied to elute peptides. The ESI-IT MS was operated in positive ion mode over the range of 350–2000 (m/z) and the database search was carried out against the IPI Human using MASCOT (Matrixscience). The following search parameters were used: the cutting enzyme, trypsin; one missed cleavage allowed, mass tolerance window, ±1 Da, the MS/MS tolerance window, ±0.8 Da; carbamidomethyl cystein and oxidized methionine as fixed and variable modifications, respectively.

Detection of phosphorylated peptide. Possible phosphorylation sites were investigated by MALDI-TOF-MS using monoammonium phosphate (MAP) added matrix mainly according to Nabetani et al. [21]. An additive of MAP was mixed with α-CHCA matrix solution (5 mg/mL, 0.1% TFA, 50% ACN aqueous) to 40 mM in final concentration. Tryptsin digests of the spots positively stained with ProQ were dissolved into 4 μL of 0.1% TFA, 50% ACN aqueous solution and 1 μL of the peptides solution was spotted on the MALDI target plate. After drying up, 1 μL of the MAP matrix was dropped on the dried peptide mixture. Voyager DE-STR (ABI) was used to obtain mass spectra both in negative and positive ion mode. MS peaks that had relatively stronger intensities in negative ion mode than in positive ion mode were selected as candidates for acidically modified peptides.

Results and discussion

We identified 195 spots representing 125 proteins (Suppl. Table 1) and obtained the corresponding mRNA expression data for a total of 93 proteins (149 spots) (Suppl. Table 2). These 93 proteins were classified according to their biological processes and subcellular localizations into categories described by the Gene Ontology Consortium (http://www.geneontology.org/index.shtml) and about a half of them were related to metabolic processes (Fig. 1A). It is a general agreement that proteins with extremely high or low p*I* as well as hydrophobic proteins are difficult to be detected by 2-DE. Being consistent with this notion, our analysis detected many cytoplasmic proteins (Fig. 1B). Therefore, the protein expression data presented here were biased in favor of cytoplasmic and soluble proteins. The protein expression abundance between non-HCC and HCC was calculated using the normalized spot volume, which was the ratio of spot volume relative to IS (Cy3:Cy2 or Cy5:Cy2) and we used the Student's paired *t*-test ($p < 0.05$) to select the protein spots which were expressed differentially between non-HCC and HCC, using 2-DE gel images run in triplicate. The spot volume of a multi-spotted protein was indicated as a total volume by integrating the intensities of multiple spots as was done by Gygi et al. [10]. Comparison of protein expression profiles revealed that several proteins were expressed differentially between HCC and non-HCC. Proteins whose abundances increased >2-fold or decreased <1/2 in HCC are listed in Table 2. While glutamine synthetase, vimentin, annexin A2 and aldo-keto reductase were up-regulated, carbonic anhydrase 2, argininosuccinate synthetase 1, carbonic anhydrase 1, fructose-1,6-bisphosphatase 1, and betaine-homocysteine methyltransferase were down-regulated in HCC. Up- or down-regulation of most of these proteins in HCC has been reported previously [22–27]. Up-regulation of vimentin and annexin A2, and reduced expression of carbonic anhydrase 1 and 2 was suspected to be associated with cellular motility and metastasis [23,24,26].

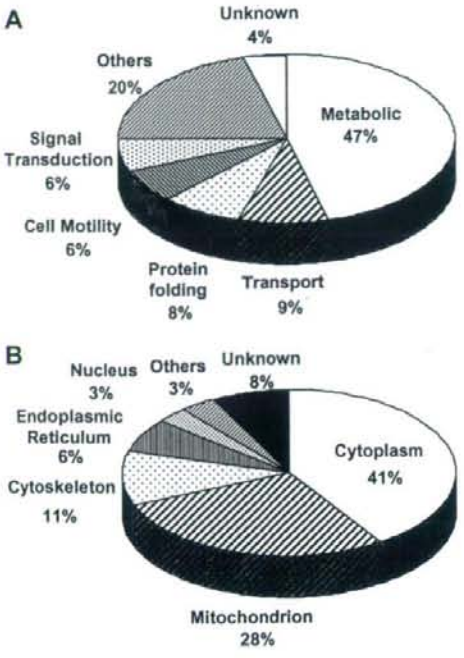

Fig. 1. Classification of identified proteins according to their cellular function (A) and subcellular localization (B).

The mRNA expression abundance was calculated from cDNA microarray data. Hierarchical clustering of

Table 2
Proteins expressed differentially between HCC and non-HCC

Spot ID	Protein name	Refseq ID	Theoretical		Fold change (HCC/non-HCC)		References
			p*I*	MW (kDa)	Protein[a]	mRNA	
1353, 1354	Glutamine synthase	NP_002056.2	6.43	42.7	2.06	3.08	[22]
1039, 1046	Vimentin	NP_003371	5.09	53.6	2.30	1.51	[23]
1716	Annexin A2	NP_001002857.1	7.57	38.8	2.57	1.82	[24]
1685, 1699	Aldo-keto reductase 1B10	NP_064695	7.12	36.2	4.29	4.73	[25]
1977	Carbonic anhydrase 2	NP_000058	6.87	29.3	0.39	0.62	[26]
1307, 1312, 1331	Argininosuccinate synthetase 1	NP_000041.2	8.08	46.8	0.41	0.30	[27]
1941	Carbonic anhydrase 1	NP_001729	6.59	28.9	0.47	1.25	[26]
1582	Fructose-1,6-bisphosphatase 1	NP_000498	6.54	37.2	0.48	0.36	
1256	Betaine-homocysteine methyltransferase	NP_001704	6.41	45.4	0.48	0.40	

[a] Integrated spot volume was used to calculate the fold change of multi-spotted proteins.

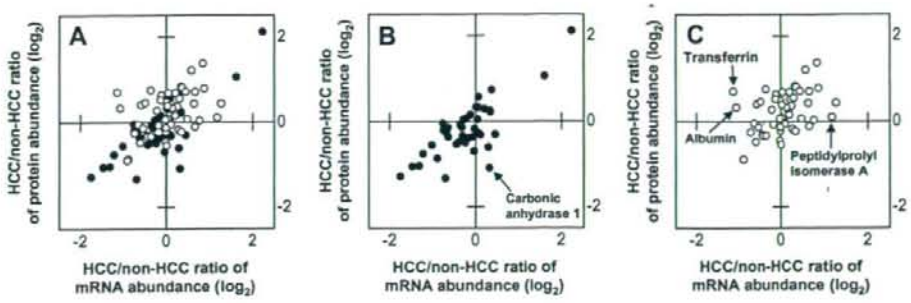

Fig. 2. Comparative analysis of protein and mRNA expression profiles between HCC and non-HCC. (A) The HCC/non-HCC ratios of averaged protein expression levels for 93 proteins were plotted against those of mRNA. Proteins related to metabolic pathways were indicated in closed circles and were shown again in (B). Proteins related to the other biochemical pathways were indicated in open circles and shown in (C). Proteins listed in Table 3 were indicated in (B) and (C). All graphs were depicted in $\log_2$ scale.

Table 3
Proteins whose expression changes between HCC and non-HCC show poor correlation to mRNA expression changes

Spot ID	Protein name	Refseq ID	Theoretical		Spot[a] Av. Ratio	Spot *p* value	Protein ratio	Micro array Av. ratio	Micro array *p* value
			*p*I	MW (kDa)					
564	Transferrin	NP_001054	6.8	79.3	2.23	0.035	1.61	0.45	3.3E−06
565					1.87	0.079			
566					2.28	0.13			
605					0.73	0.098			
1489	Albumin	NP_000468	5.9	71.3	—	0.63	1.25	0.47	2.3E−03
1941	Carbonic anhydrase 1	NP_001729	6.6	28.9	—	3.5E−03	0.47	1.25	0.39
2290	Peptidylprolyl isomerase A	NP_066953	7.7	18.1	—	5.0E−01	1.07	2.29	1.1E−01

[a] Since transferrin was detected in multiple spots, averaged ratio and spot *p* value of each spot is shown.

Table 4
Multi-spotted proteins showing spot-to-spot differences in expression level between non-HCC and HCC

Spot ID	Spot Av. ratio	Spot *p* value	Protein name	Refseq ID	Theoretical		Protein[a] ratio
					*p*I	MW (kDa)	
436	1.92	5.3E−04	Tumor rejection antigen (gp96)	NP_003290	4.8	92.7	1.2
537	0.79	0.16					
564	2.23	0.035	Transferrin	NP_001054	6.8	79.3	1.61
565	1.87	0.079					
566	2.28	0.13					
605	0.73	0.098					
1257	1.02	0.92	Fumarate hydratase	NP_000134	8.8	54.8	0.8
1261	0.6	1.3E−03					

[a] HCC/non-HCC protein ratios were calculated using integrated spot abundances.

gene expression was done with BRB-ArrayTools (http://linus.nci.nih.gov/BRB-ArrayTools.htm). The filtered data were log-transferred, normalized, centered, and applied to the average linkage clustering with centered correlation. BRB-ArrayTools contains a class comparison tool based on univariate *F* tests to find genes differentially expressed between predefined clinical groups. The permutation distribution of the *F* statistic, based on 2000 random permutations, was also used to confirm statistical significance. A *p* value of less than 0.05 for differences in HCC/non-HCC gene expression ratio was considered significant.

The average HCC/non-HCC expression ratios of the 93 proteins were plotted against the mRNA ratios in Fig. 2, where a positive value indicates increased expression in HCC and a negative ratio indicates reduced expression. The overall expression ratio of HCC/non-HCC indicated noticeable correlation between protein and mRNA

(Fig. 2A), and the Pearson's correlation coefficient for this data set (93 proteins/genes) was 0.73. Next, we divided 93 proteins into those related to metabolism and others biological processes. The HCC/non-HCC ratios of protein expression for metabolism-related proteins showed substantial correlation with those of mRNA (Fig. 2B, $r = 0.9$), whereas those of other proteins were poorly correlated (Fig. 2C, $r = 0.36$). Extreme care must be taken in a direct comparison of proteomic data with transcriptome because of multiple layers of discrepancies caused by the distinct sensitivities of cDNA array hybridization and 2-DE, the inability of a cDNA array to distinguish mRNA isoforms and post-translational modifications of proteins. Nevertheless, our results suggest that the expression of considerable portion of proteins with metabolic function listed here is regulated at transcriptional level. On the other hand, post-transcriptional and/or post-translational processes seem to be involved in the regulation of expression level for proteins with other cellular functions as a whole. Four proteins (albumin, transferrin, peptidylproryl isomerase A, and carbonic anhydrase 1) showed apparent poor correlation in protein and mRNA expression profiles (Table 3 and Fig. 2). Transcriptional control might have little effect on the expression changes of these proteins between HCC and non-HCC.

A number of proteins were expressed as multiple spots on 2-DE gels and most multi-spotted proteins showed little spot-to-spot variations in the averaged HCC/non-HCC ratio. Although we do not know how these multiple spots were generated, many of them might be due to the conformational equilibrium of proteins under electrophoresis rather than to any post-translational modifications [28]. On the other hand, the HCC/non-HCC expression ratios of several multi-spotted proteins varied from spot to spot, and three proteins (transferrin, fumarate hydratase, and tumor rejection antigen gp96) were categorized as these multi-spotted proteins (Table 4).

For example, gp96 was detected in two spots (spot #436 and 537) with distinct molecular mass and p*I* and they showed different HCC/non-HCC expression ratio (Fig. 3A and B and Table 4). The expression of these two isoforms was observed to change in the opposite direction between non-HCC and HCC: #436 was up-regulated in HCC (HCC/non-HCC ratio: 1.96) while #537 was down-regulated (HCC/non-HCC ratio: 0.79) (Table 4 and Fig. 3C and D). Gp96 is a glycoprotein present in endoplasmic reticulum and is supposed to function as a molec-

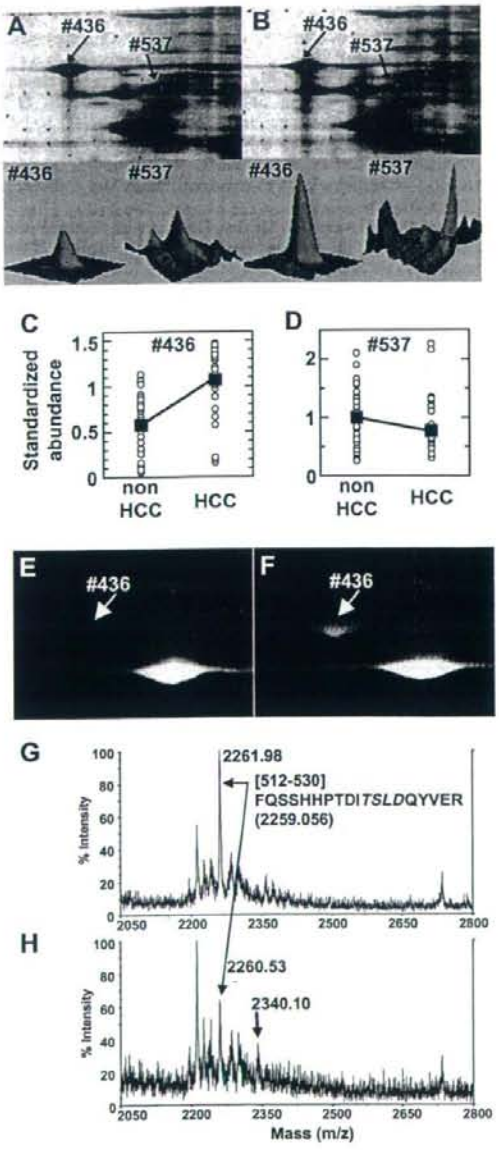

Fig. 3. Comparison of expression profiles of two gp96 spots between HCC and non-HCC. The expression profile and phosphorylation of tumor rejection antigen gp96 in HCC and non-HCC was investigated. Magnified gel images and 3D views of two gp96 spots in non-HCC (A) and HCC (B) were shown. Differences in expression level of two gp96 spots, #436 (C) and #537 (D), between non-HCC and HCC were shown. The open circle indicates the standardized abundance of the individual spot in each sample. The closed square represents the averaged abundance of each gp96 spot. Magnified gel images of non-HCC (E) and HCC (F) stained with ProQ. The #436 spot was positively stained with ProQ, while unambiguous staining of the #537 spot was not observed. Tryptic peptides prepared from the spot #436 were analyzed by MALDI–TOF mass-spectrometry in the positive ion mode (G) and the negative ion mode (H). A peak of 2261.98 detected in positive ion mode corresponds to the amino acid sequence from 512 to 530. In addition to the original peak (*m/z*: 2260.53), a peak mass shifted by +80 Da was detected in the negative ion mode. A predicted phosphorylation consensus motif for protein kinase CK2 is indicated in italics (G).

ular chaperone and intracellular Ca^{2+} regulator [29,30]. Several previous reports have shown that gp96 is glycosylated and phosphorylated, and exists as heterogeneous molecular entities with various molecular weights [31]. In order to know whether gp96 spots were phosphorylated or not, we stained the 2-DE gels with ProQ Diamond which is a dye specific to proteins phosphorylated on serine, threonine or tyrosine residues [32], and has been used successfully to visualize phosphoproteins [33]. We found that the spot #436 was positively stained with ProQ (Fig. 3E and F). We further tried to detect possible phosphorylated peptides in the tryptic digests prepared from #436 by MALDI–TOF–MS according to Nabetani et al. [21]. Searching for those peaks that had relatively stronger intensities in negative ion mode than in positive ion mode, we found two peaks as candidates for acidically modified peptides. They were assigned to the peptides SILFVPTSAPR (amino acid sequence: 385–395, data not shown) and FQSSHHPTDITSLDQYVER (aa512–530). Fig. 3G and H show the unmodified peak and the acidically modified peak (mass shifted by +80 Da in negative ion mode) of the latter peptide, respectively. This peptide contained a predicted phosphorylation consensus motif, [Ser or Thr]-X-X-[Asp or Glu], for protein kinase CK2 (Fig. 3G) which was suggested to phosphorylate gp96 [34]. These results together with ProQ staining indicated that at least one gp96 isoform was phosphorylated and was up-regulated in HCC. Over-expression of gp96 in HCC has been reported previously [35], though the reports that showed over-expression of its phosphorylated form are rare. Further investigation into biological meaning of gp96 phosphorylation may provide us important information about HCC development.

Acknowledgments

We thank the late Dr. A. Tsugita for helpful discussion through this work and N. Tetsura for technical assistance.

Appendix A. Supplementary data

Supplementary data associated with this article can be found, in the online version, at doi:10.1016/j.bbrc.2007.11.101.

References

[1] T.K. Seow, R.C.M.Y. Liang, C.K. Leow, M.C.M. Chung, Hepatocellular carcinoma: from bedside to proteomics, Proteomics 1 (2001) 1249–1263.
[2] L.J. Lopez, J.A. Marrero, Hepatocellular carcinoma, Curr. Opin. Gastroenterol. 3 (2004) 248–253.
[3] H.F. Kawai, S. Kaneko, M. Honda, Y. Shirota, K. Kobayashi, Alpha-fetoprotein-producing hepatoma cell lines share common expression profiles of genes in various categories demonstrated by cDNA microarray analysis, Hepatology 3 (2001) 676–691.
[4] N. Iizuka, M. Oka, H. Yamada-Okabe, N. Mori, T. Tamesa, T. Okada, N. Takemoto, K. Hashimoto, et al., Differential gene expression in distinct virologic types of hepatocellular carcinoma: association with liver cirrhosis, Oncogene 22 (2003) 3007–3014.
[5] T. Yamashita, S. Kaneko, S. Hashimoto, T. Sato, S. Nagai, N. Toyoda, T. Suzuki, K. Kobayashi, et al., Serial analysis of gene expression in chronic hepatitis C and hepatocellular carcinoma, Biochem. Biophys. Res. Commun. 282 (2001) 647–654.
[6] K. Kawaguchi, M. Honda, T. Yamashita, Y. Shirota, S. Kaneko, Differential gene alteration among hepatoma cell lines demonstrated by cDNA microarray-based comparative genomic hybridization, Biochem. Biophys. Res. Commun. 329 (2005) 370–380.
[7] Y. Midorikawa, M. Makuuchi, W. Tang, H. Aburatani, Microarray-based analysis for hepatocellular carcinoma: from gene expression profiling to new challenges, World J. Gastroenterol. 13 (2007) 1487–1492.
[8] N.A. Shackel, D. Seth, P.S. Haber, M.D. Gorrell, G.W. McCaughan, The hepatic transcriptome in human liver disease, Comp. Hepatol. 5 (6) (2006).
[9] T.J. Griffin, S.P. Gygi, T. Ideker, B. Rist, J. Eng, L. Hood, R. Aebersold, Complementary profiling of gene expression at the transcriptome and proteome levels in *Saccharomyces cerevisiae*, Mol. Cell. Proteomics 4 (2002) 323–333.
[10] S.P. Gygi, Y. Rochon, B.R. Franza, R. Aebersold, Correlation between protein and mRNA abundance in yeast, Mol. Cell. Biol. 19 (1999) 1720–1730.
[11] M. Unlu, M.E. Morgan, J.S. Minden, Difference gel electrophoresis: a single gel method for detecting changes in protein extracts, Electrophoresis 11 (1997) 2071–2077.
[12] I.N. Lee, C.H. Chen, J.C. Sheu, H.S. Lee, G.T. Huang, C.Y. Yu, F.J. Lu, L.P. Chow, Identification of human hepatocellular carcinoma-related biomarkers by two-dimensional difference gel electrophoresis and mass spectrometry, J. Proteome Res. 6 (2005) 2062–2069.
[13] C.R. Liang, C.K. Leow, J.C. Neo, G.S. Tan, S.L. Lo, J.W. Lim, T.K. Seow, P.B. Lai, et al., Proteome analysis of human hepatocellular carcinoma tissues by two-dimensional difference gel electrophoresis and mass spectrometry, Proteomics 5 (2005) 2258–2271.
[14] V.J. Desmet, M. Gerber, J.H. Hoofnagle, M. Manns, P.J. Scheuer, Classification of chronic hepatitis: diagnosis, grading and staging, Hepatology 19 (1994) 1513–1520.
[15] K.G. Ishak, P.P. Anthony, L.H. Sobin, Histological typing of tumours of the liver, 2nd ed.WHO International Histological Classification of Tumors, Springer-Verlag, New York, 1994.
[16] M. Honda, S. Kaneko, H. Kawai, Y. Shirota, K. Kobayashi, Differential gene expression between chronic hepatitis B and C hepatic lesion, Gastroenterology 120 (2001) 955–966.
[17] H.F. Kawai, S. Kaneko, M. Honda, Y. Shirota, K. Kobayashi, Alpha-fetoprotein-producing hepatoma cell lines share common expression profiles of genes in various categories demonstrated by cDNA microarray analysis, Hepatology 33 (2001) 676–691.
[18] M. Honda, H. Kawai, Y. Shirota, T. Yamashita, T. Takamura, S. Kaneko, cDNA microarray analysis of autoimmune hepatitis, primary biliary cirrhosis and consecutive disease manifestation, J. Autoimmun. 25 (2005) 133–140.
[19] M. Honda, T. Yamashita, T. Ueda, H. Takatori, R. Nishino, S. Kaneko, Different signaling pathways in the livers of patients with chronic hepatitis B or chronic hepatitis C, Hepatology 44 (2006) 1122–1138.
[20] Y. Tabuse, T. Nabetani, A. Tsugita, Proteomic analysis of protein expression profiles during *Caenorhabditis elegans* development using 2D-difference gel electrophores, Proteomics 5 (2005) 2876–2891.
[21] T. Nabetani, K. Miyazaki, Y. Tabuse, A. Tsugita, Analysis of acidic peptides with a matrix-assisted laser desorption/ionization mass spectrometry using positive and negative ion modes with additive monoammonium phosphate, Proteomics 6 (2006) 4456–4465.
[22] Y. Kuramitsu, T. Harada, M. Takashima, Y. Yokoyama, I. Hidaka, N. Iizuka, T. Toda, M. Fujimoto, et al., Increased expression and phosphorylation of liver glutamine synthetase in well-differentiated

hepatocellular carcinoma tissues from patients infected with hepatitis C virus, Electrophoresis 27 (2006) 1651–1658.
[23] L. Hu, S.H. Lau, C.H. Tzang, J.M. Wen, W. Wang, D. Xie, M. Huang, Y. Wang, et al., Association of Vimentin overexpression and hepatocellular carcinoma metastasis, Oncogene 23 (2004) 298–302.
[24] Z. Dai, Y.K. Liu, J.F. Cui, H.L. Shen, J. Chen, R.X. Sun, Y. Zhang, X.W. Zhou, Identification and analysis of altered alpha1,6-fucosylated glycoproteins associated with hepatocellular carcinoma metastasis, Proteomics 6 (2006) 5857–5867.
[25] E. Zeindl-Eberhart, S. Haraida, S. Liebmann, P.R. Jungblut, S. Lamer, D. Mayer, G. Jäger, S. Chung, H.M. Rabes, Detection and identification of tumor-associated protein variants in human hepatocellular carcinomas, Hepatology 39 (2004) 540–549.
[26] W.H. Kuo, W.L. Chiang, S.F. Yang, K.T. Yeh, C.M. Yeh, Y.S. Hsieh, S.C. Chu, The differential expression of cytosolic carbonic anhydrase in human hepatocellular carcinoma, Life Sci. 73 (2003) 2211–2223.
[27] P.N. Cheng, T.L. Lam, W.M. Lam, S.M. Tsui, A.W. Cheng, W.H. Lo, Y.C. Leung, Pegylated recombinant human arginase (rhArg-peg5,000mw) inhibits the in vitro and in vivo proliferation of human hepatocellular carcinoma through arginine depletion, Cancer Res. 67 (2007) 309–317.
[28] F.S. Berven, O.A. Karisen, J.C. Murrell, H.B. Jensen, Multiple polypeptide forms observed in two-dimensional gels of Methylococcus capsulatus (Bath) polypeptides are generated during the separation procedure, Electrophoresis 24 (2003) 757–761.
[29] J. Melnick, S. Aviel, Y. Argon, The endoplasmic reticulum stress protein GRP94, in addition to BiP, associates with unassembled immunoglobulin chains, J. Biol. Chem. 267 (1992) 21303–21306.
[30] H. Liu, E. Miller, B. van de Water, J.L. Stevens, Endoplasmic reticulum stress proteins block oxidant-induced Ca^{2+} increases and cell death, J. Biol. Chem. 273 (1998) 12858–12862.
[31] A.M. Feldweg, P.K. Srivastava, Molecular heterogeneity of tumor rejection antigen/heat shock protein GP96, Int. J. Cancer 63 (1995) 310–314.
[32] T.H. Steinberg, B.J. Agnew, K.R. Gee, W.-Y. Leung, T. Goodman, B. Schulenberg, J. Hendrickson, J.M. Beechem, R.P. Haugland, W.F. Patton, Global quantitative phosphoprotein analysis using multiplexed proteomics technology, Proteomics 3 (2003) 1128–1144.
[33] B.R. Chitteti, Z. Peng, Proteome and phosphoproteome dynamic change during cell dedifferentiation in Arabidopsis, Proteomics 7 (2007) 1473–1500.
[34] S.E. Cala, GRP94 hyperglycosylation and phosphorylation in Sf21 cells, Biochim. Biophys. Acta 1496 (2000) 296–310.
[35] D.F. Yao, X.H. Wu, X.Q. Su, M. Yao, W. Wu, L.W. Qiu, L. Zou, X.Y. Meng, Abnormal expression of HSP gp96 associated with HBV replication in human hepatocellular carcinoma, Hepatobiliary Pancreat. Dis. Int. 5 (2006) 381–386.

ELSEVIER

Journal of Hepatology 49 (2008) 779–786

Journal of Hepatology

www.elsevier.com/locate/jhep

Decreased expressions of CD1d molecule on liver dendritic cells in subcutaneous tumor bearing mice☆

Tomohide Tatsumi[1,2,3], Tetsuo Takehara[1,3], Shinjiro Yamaguchi[1,3], Akira Sasakawa[1,3], Masashi Yamamoto[1,3], Yui Fujita[1], Takuya Miyagi[1], Kazuyoshi Ohkawa[1], Norio Hayashi[1,3,*]

[1]*Department of Gastroenterology and Hepatology, Osaka University Graduate School of Medicine, 2-2 Yamadaoka, Suita, Osaka 565-0871, Japan*
[2]*Medical Center for Translational Research, Osaka University Hospital, Osaka 565-0871, Japan*
[3]*Core Research for Evolutional Science and Technology (CREST), Japan Science and Technology Agency (JST), Tokyo 150-0002, Japan*

***Background/Aims*: α-Galactosylceramide (α-GalCer) has been attracting attention as a novel approach to treat metastatic liver cancer. However, the activation of liver innate immunity by α-GalCer should be examined because clinical trials of α-GalCer resulted in limited clinical responses.**

***Methods*: We examined the activation of liver innate immunity by α-GalCer in subcutaneous Colon26 tumor bearing-mice (C26s.c.TB-mice).**

***Results*: The expressions of CD1d molecule on liver dendritic cells (DCs) were significantly lower in C26s.c.TB-mice than those in tumor-unbearing normal mice. Although liver NK cells and NKT cells activated in normal mice after α-GalCer treatment, the activation of these cells were significantly inhibited in C26s.c.TB-mice. α-GalCer treatment resulted in significant antitumor effect against Colon26 metastatic liver tumor in normal mice, but not in C26s.c.TB-mice. The serum levels of TGF-β, known to suppress the CD1d expressions on DCs, in C26s.c.TB-mice were significantly higher than those in normal mice. Surgical subcutaneous tumor mass reduction resulted in the reduction of serum TGF-β, the recovery of CD1d expressions on liver DCs and the improvement of antitumor effect of α-GalCer against metastatic liver tumor.**

***Conclusions*: These results suggested that tumor burden reduces CD1d expressions on liver DCs, thus impeding α-GalCer-mediated NK cell activation and antitumor activity in the liver.**

***Keywords*: α-Galactosylceramide; CD1d; Liver dendritic cells; Antitumor immunity**

1. Introduction

The glycolipid antigen α-galactosylceramide (α-GalCer) induces activation of NKT cells in a CD1d-dependent manner [1]. α-GalCer presented by DCs efficiently stimulates NKT cells implicated in the innate immunity [2,3]. Recently α-GalCer has been attracting attention for novel anti-tumor therapy. *In vivo* animal studies have shown that systemic administration of α-GalCer can lead to anti-tumor effects against metastatic liver tumor [4,5], suggesting that α-GalCer treatment might be promising for clinical application against liver tumor. Metastatic liver tumors, one of the most common types of advanced malignancy, resist conventional chemotherapy and radiotherapy, and present with a poor prognosis. Thus novel and more effective immunotherapy is needed, especially for metastatic liver cancer. Several phase I clinical studies have been carried

Received 29 February 2008; received in revised form 11 June 2008; accepted 14 June 2008; available online 2 July 2008
Associate Editor: V. Barnaba

☆ The authors declare that they do not have anything to disclose regarding funding from industries or conflict of interest with respect to this manuscript.

* Corresponding author. Fax: +81 6 6879 3629.
E-mail address: hayashin@gh.med.osaka-u.ac.jp (N. Hayashi).

Abbreviations: DC, dendritic cell; APC, antigen-presenting cells; CTL, cytotoxic T lymphocytes; α-GalCer, α-galactosylceramide; M-NC, mononuclear cells; TB, tumor bearing.

0168-8278/$34.00 © 2008 Published by Elsevier B.V. on behalf of the European Association for the Study of the Liver.
doi:10.1016/j.jhep.2008.06.011

out in cancer immunotherapy using intravenous administration of α-GalCer, but with limited clinical responses [6,7]. Most clinical trials of cancer immunotherapy have been conducted with patients at advanced stages of cancer. Thus, for further development of α-GalCer treatment in such patients, the antitumor effect of α-GalCer should be examined in hosts with an advanced tumor burden.

In the current study, we evaluated the anti-tumor effect of administration of α-GalCer against liver tumor in subcutaneous tumor bearing animals. Both the antitumor effect of α-GalCer against liver tumor and liver NK cell and NKT cells activation were impaired in subcutaneous tumor bearing mice (s.c.TB-mice). The liver DCs were poorly activated by α-GalCer administration with lower expression of CD1d, NKT-activating molecules. However, the CD1d expression increased and the antitumor effect of α-GalCer against liver tumor was improved after surgical resection of the subcutaneous tumor mass. Our study has shed light toward understanding of the antitumor effect of α-GalCer in metasatic liver cancer patients.

2. Materials and methods

2.1. Mice

Six-to-eight week old female BALB/c mice were purchased from Shizuoka Experimental Animal Laboratory (Shizuoka, Japan), and maintained in micro-isolator cages. The animals were handled under aseptic conditions. Procedures were performed according to approved protocols and in accordance with recommendations for the proper care and use of laboratory animals.

2.2. Cell lines

Colon26, a mouse colon adenocarcinoma cell line was kindly provided by Dr. Takashi Tsuruo (Institute of Molecular and Cellular Bioscience, The University of Tokyo, Tokyo, Japan). This cell line was maintained in complete medium (CM, RPMI-1640 medium supplemented with 10% heat-inactivated fetal bovine serum, 100 U/ml penicillin, 100 μg/ml streptomycin and 10 mM L-glutamine: all reagents from GIBCO/Life Technologies, Grand Island, New York) in a humidified incubator at 5% CO_2 and 37 °C.

2.3. α-GalCer

α-GalCer was kindly provided by Kirin Pharma Co. Ltd. (Gunma, Japan) and prepared as previously described [8].

2.4. Animal experiments

To establish Colon26 s.c.TB-mice (C26s.c.TB-mice), BALB/c mice were subcutaneously injected with 3×10^6 Colon26. On day 42, when the tumor size reached approximately 200 mm^2, bone marrow-derived DCs (BM-DCs) and liver DCs were prepared to evaluate the CD1d expression in C26s.c.TB-mice. BM-DC were generated as previously described [8]. Hepatic mononuclear cells (MNC) were prepared as previously described [8]. CD11c+ dendritic cells were isolated from hepatic MNC by magnetic cell sorting using MACS (Miltenyi Biotec, Gladbach, Germany) according to the manufacturer's protocol.

Hepatic metastasis of Colon26 cells was established as previously described [9]. To examine antitumor effect of α-GalCer in the liver of C26s.c.TB-mice, C26s.c.TB-mice or normal mice were injected with 5×10^5 Colon26 cells into the spleen 42 days after mice were subcutaneously injected with 3×10^6 Colon26 cells. Twenty-four hours later, α-GalCer (2 μg/100 μl) or 100 μl of the vehicle was administered intraperitoneally to each mouse. Ten days after tumor injection, the livers of the treated mice were removed, and the liver weight was measured to examine intrahepatic tumor growth.

2.5. Flow cytometry

For phenotypic analysis of BM-DCs and liver DCs, PE- or FITC-conjugated monoclonal antibodies (Ab) against mouse cell surface molecules [CD1d, CD80, CD86 CD11c (all from BD-Pharmingen, San Diego, CA), MHC class II (Miltenyi Biotec)], and appropriate isotype controls were used. We defined DCs with CD11c+ MHC class II+ cells by flow cytometry. To detect the NK cell and NKT cell population in liver MNCs, MNC were stained with PE-conjugated DX5 Ab and FITC-conjugated TCRβ (all from BD-Pharmingen). C26s.c.TB-mice and normal mice were injected intraperitoneally with α-GalCer (2 μg/100 μl) or 100 μl of vehicle. Hepatic MNC were prepared on day 0, 1, 3 and 7 after α-GalCer injection, and both NK cell and NKT cell populations in hepatic MNC were evaluated by flow cytometry. Flow cytometric analysis was performed using a FACscan (Becton Dickinson, San Jose, CA) flow cytometer. The results of flow cytometric analysis are reported in arbitrary mean fluorescence intensity (MFI) units.

2.6. TGF-β and IL-10 ELISA

Mice sera from C26s.c.TB-mice were harvested 42 days after intrahepatic tumor injection. Mice sera and the culture supernatants of Colon26 cells were subjected to mouse TGF-β ELISA (R&D systems, Minneapolis, MN) and mouse IL-10 ELISA (BD-Pharmingen), with lower levels of detection of 31.2 and 31.3 pg/ml, respectively.

2.7. Cytotoxic assay

To evaluate the activation of liver NK cells in C26s.c.TB-mice treated with α-GalCer, liver MNC were isolated 48 h after α-GalCer injection and subjected to ^{51}Cr release assay against NK-susceptible YAC-1 target as previously described [4]. Assays were performed in triplicate, with spontaneous release of all assays not exceeding 25% of the maximum release.

2.8. Surgical resection of subcutaneous tumor

To assess the impact of subcutaneous tumor on the CD1d expression of liver DCs, subcutaneous Colon26 tumors were surgically resected on day 42 after subcutaneous injection of Colon26 cells (C26s.c.TB-ope mice). Fourteen days after subcutaneous tumor resection, liver DCs were isolated and subjected to flow cytometry to evaluate the CD1d expression. To examine antitumor effect of α-GalCer in the liver of C26s.c.TB-ope mice, C26s.c.TB-mice or C26s.c.TB-ope mice were injected with 5×10^5 Colon26 cells into the spleen 10 days after subcutaneous tumor resection. Twenty-four hours later, α-GalCer (2 μg/100 μl) was administered intraperitoneally as above. Ten days later, the livers of the treated mice were removed, and the liver weights were measured to examine intrahepatic tumor growth.

2.9. Statistical analysis

The statistical significance of differences between the groups was determined by applying compared t test with Welch correction or Mann–Whitney U test. The statistical significance of the differences in more than three groups was determined by applying one-way ANOVA. We defined statistical significance as $p < 0.05$.

3. Results

3.1. Expressions of CD1d on DCs in C26s.c.TB-mice were lower than those in normal mice

Since α-GalCer induces activation of NKT cells in a CD1d-dependent manner [1], the expression of CD1d plays an important role in the activation of NKT cells. We examined the CD1d expressions on DCs in C26s.c.TB-mice. The expressions of CD1d on BM-DCs were similar in both normal and C26s.c.TB-mice (Fig. 1A and B). In contrast, those on liver DCs from C26s.c.TB-mice were significantly lower than those from normal mice (Fig. 1A and C). Spleen DCs from C26s.c.TB-mice were also significantly lower than those from normal mice (Fig. 1A and D). These results demonstrated that systemic decrease of CD1d expressions on DCs in each organ is observed in C26s.c.TB-mice, but the potential of differentiation of CD1d expressing DCs from precursor cells in bone marrow was similar between in C26s.c.TB-mice and normal mice.

3.2. The activation of liver NK cells, liver NKT cells and liver DCs was impaired in C26s.c.TB-mice

We next examined the activation of liver NK cells and liver NKT cells in C26s.c.TB-mice after administration of α-GalCer. The cytolytic activity of liver NK cells in α-GalCer-treated mice was stronger than that in vehicle-treated mice in normal mice. In marked contrast, the cytolytic activities in both α-GalCer and vehicle-treated mice were very weak in C26s.c.TB-mice (Fig. 2A). In normal mice, the liver NK cell proportions in whole liver MNCs increased with the peak at 1 day after α-

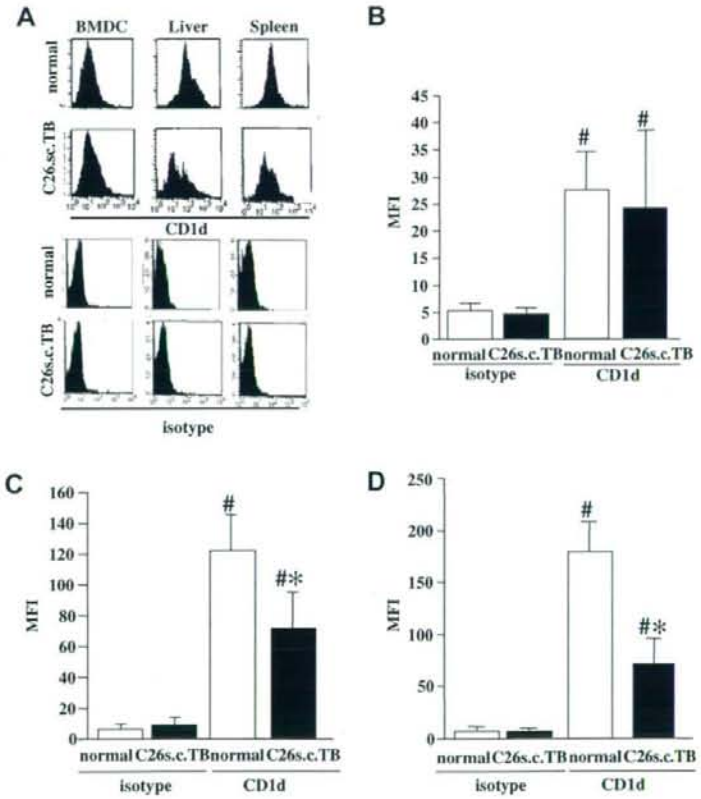

Fig. 1. CD1d expression on DCs in C26s.c.TB-mice. BM-DCs, liver and spleen DCs were prepared from C26s.c.TB-mice or normal mice ($N = 3$ in each group), and the expressions of CD1d molecules on DCs were evaluated by flow cytometry. The representative flow cytometry data of CD1d expressions on BM-DCs, liver DCs and spleen DCs were shown in Fig. 1A. The expression levels of CD1d molecules are reported in arbitrary MFI (mean ± SD). Normal: MFI of DCs from normal mice stained with anti-CD1d or isotype control antibody. C26s.c.TB: MFI of DCs from C26s.c.TB-mice stained with anti-CD1d or isotype control antibody. The CD1d expression on BM-DCs (B), on liver DCs (C), on spleen DCs (D). $^{\#}p < 0.05$ vs. respective isotype control $^{*}p < 0.05$ vs. CD1d expression in normal mice.

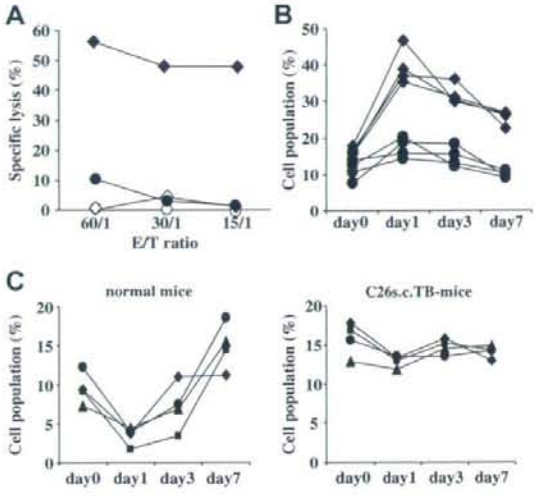

Fig. 2. Impaired activation of liver NK cells and NKT cells in C26s.c.TB-mice. (A) To evaluate the activation of liver NK cells in C26s.c.TB-mice treated by α-GalCer, liver MNC were isolated 48 h after α-GalCer injection and were subjected to ^{51}Cr release assay against NK-susceptible YAC-1 target. (♦) α-GalCer-treated normal mice, (◇) vehicle-treated normal mice, (•) α-GalCer-treated C26s.c.TB-mice, (○) vehicle-treated C26s.c.TB-mice. Representative data shown here is from three independent experiments. (B, C) BALB/c normal mice or C26s.c.TB-mice were injected intraperitoneally with α-GalCer. Hepatic MNC were prepared on day 0, 1, 3 and 7 days after α-GalCer injection. Liver NK cell and NKT cell populations in hepatic MNC were evaluated by flow cytometry. (B) Liver NK cell populations (DX5+/TCRβ− cells) in hepatic MNC after α-GalCer treatment. (♦) NK cell in each normal mice, (•) NK cell in each C26s.c.TB-mice ($N = 4$ in each group). (C) Liver NKT cell populations (DX5+/TCRβ+ cells) in hepatic MNC after α-GalCer treatment in normal mice and C26s.c.TB-mice ($N = 4$ in each group).

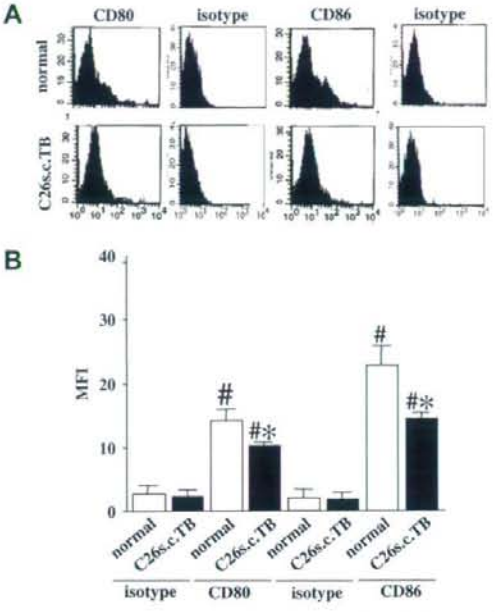

Fig. 3. The CD80 and CD86 expressions of liver DCs in C26s.c.TB-mice and normal mice. The expressions of CD80 and CD86 on liver DCs from both normal mice and C26s.c.TB-mice were evaluated by flow cytometry ($N = 3$ in each group). The representative flow cytometry data of CD80 and CD86 expressions on liver DC were shown in Fig. 3A. The expression levels of CD80 and CD86 molecules are reported as arbitrary MFI (mean ± SD of triplicate samples, Fig. 3B). $^{\#}p < 0.05$ vs. respective isotype control $^{*}p < 0.05$ vs. CD80 or CD86 expressions in normal mice.

GalCer administration, and the liver NK cell proportion at 7 days gradually decreased (Fig. 2B). C26s.c.TB-mice showed weaker increase of liver NK cell proportions in whole liver MNCs than normal mice (Fig. 2B). The liver NKT cell proportion decreased on day 1 and increased again on day 3 and day 7 after α-GalCer administration in normal mice. In marked contrast, those did not change on day 1, day 3 and day 7 after α-GalCer administration in C26s.c.TB-mice (Fig. 2C). The liver NK cell and NKT cell proportion in vehicle-treated mice exhibited no change in both mice groups (data not shown). These results demonstrated that the activation of liver NK cells and NKT cells by α-GalCer was impaired in C26s.c.TB-mice.

We also examined the CD80 and CD86 expressions of liver DCs in both C26s.c.TB-mice and normal mice, which are indicators of the antigen-presenting function of DCs. The expressions of CD80 and CD86 molecules on liver DCs from C26s.c.TB-mice were significantly lower than those from normal mice after α-GalCer administration (Fig. 3), suggesting that the antigen-presenting function of liver DC in C26s.c.TB-mice was also impaired compared with normal mice.

3.3. The antitumor effect of α-GalCer administration against metastatic liver tumor was impaired in C26s.c.TB-mice

We examined the antitumor effect of α-GalCer administration against metastatic liver tumor in both normal and C26s.c.TB-mice. With normal mice, no tumor formation was observed in the liver of any of the α-GalCer-treated mice although large Colon26 liver tumors had formed in all vehicle-treated mice. In contrast, with the C26s.c.TB-mice, large Colon26 liver tumors had formed in both α-GalCer-treated and vehicle-treated mice. The liver weights of the α-GalCer treatment group were significantly lighter than those of the vehicle treatment group for normal mice, while they were similar for both groups of the C26s.c.TB-mice (Fig. 4). These results demonstrated that the antitumor effect of α-GalCer against metastatic liver tumor was impaired in C26s.c.TB-mice.

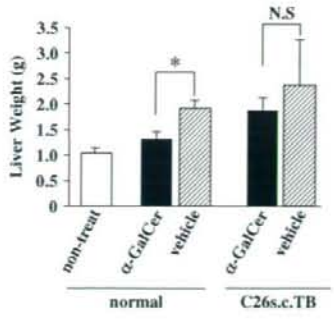

Fig. 4. Impaired antitumor effect of α-GalCer treatment against Colon26 liver tumor in C26s.c.TB-mice. To establish C26s.c.TB-mice, BALB/c mice were subcutaneously injected with 3×10^6 Colon26 cells 42 days before intrasplenic injection of tumor cells. BALB/c normal mice or C26s.c.TB-mice were injected into spleen with 5×10^5 Colon26 cells, and 24 h later either α-GalCer or vehicle was administered intraperitoneally ($N = 6$ in each treatment group). Ten days after treatment, the livers were removed from all treated mice and the liver weights of the groups were compared. As a control, the mean liver weights of untreated normal mice were 1.08 ± 0.09 g. $^*p < 0.05$. α-GalCer treatment group vs. vehicle treatment group in normal mice. N.S. α-GalCer treatment group vs. vehicle treatment group in C26s.c.TB-mice.

3.4. Serum TGF-β levels in C26s.c.TB-mice were increased compared with those in normal mice

Previous reports demonstrated that CD1d expressions on DCs decreased after co-culture with either TGF-β [10] or IL-10 [11]. The supernatants of 24 h cultures of Colon26 cells were subjected to TGF-β and IL-10 ELISA. The production of TGF-β in the supernatants of Colon26 was significantly higher than the control medium (Fig. 5A). No production of IL-10 was detected in the supernatants of Colon26 cells (data not shown). We next evaluate the serum TGF-β and IL-10 levels in C26s.c.TB-mice. The levels of TGF-β in C26s.c.TB-mice were significantly higher than that in normal mice (Fig. 5B). IL-10 was not detected in all mice sera from C26s.c.TB-mice and normal mice (data not shown).

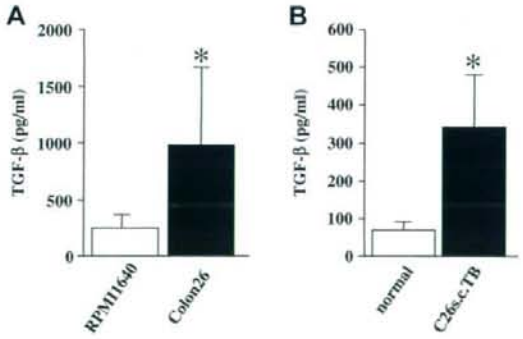

Fig. 5. The TGF-β production from Colon26 cells and the increase in serum TGF-β levels in C26s.c.TB-mice. (A) The culture supernatants of Colon26 cells or culture medium only (RPMI1640) were subjected to mouse TGF-β ELISA. (B) Mice sera from C26s.c.TB-mice were harvested 42 days after subcutaneous tumor injection and were subjected to mouse TGF-β ELISA. Mice sera from normal mice were used as controls. Cytokine levels are reported in pg/ml (mean ± SD of triplicate samples). Similar results were obtained in two independent experiments. $^*p < 0.05$.

3.5. Serum TGF-β levels decreased, the expression of CD1d molecules on liver DCs increased and the antitumor effect of α-GalCer was improved after tumor mass reduction

We next examined serum TGF-β levels and the CD1d expressions on liver DCs after surgical mass reduction in C26s.c.TB-mice. BALB/c mice were subcutaneously injected with 3×10^6 Colon26. On day 42, most Colon26 subcutaneous tumors were surgically excised (C26s.cTB-ope mice). Fourteen days later, serum TGF-β levels were evaluated, and liver DCs from C26s.c.TB-ope mice were prepared to evaluating the CD1d expression in comparison with those from C26s.c.TB-mice. The serum TGF-β levels in C26s.c.TB-ope mice were significantly lower than those in C26s.c.TB-mice (Fig. 6A). The expressions of CD1d on liver DCs from C26s.c.TB-ope mice were significantly higher than those from C26s.c.TB-mice and were similar to those from normal mice (Fig. 6B and C). These results demonstrated that surgical tumor mass reduction might lead to recovery of the impaired immune circumstances in the liver of C26s.c.TB-mice. We examined the antitumor effect of α-GalCer administration against metastatic liver tumor in both C26s.c.TB-mice and C26s.c.TB-ope mice. The liver weights of α-GalCer treated C26s.c.TB-ope mice were significantly lighter than those of α-GalCer treated C26s.c.TB-mice (Fig. 6D). These results demonstrated that the antitumor effect of α-GalCer against metastatic liver tumor was improved after subcutaneous tumor mass resection.

4. Discussion

A previous study showed that administration of α-GalCer resulted in complete rejection of Colon26 metastatic liver cancer in normal mice [5]. In the current study, we evaluated the antitumor effect of α-GalCer against the same Colon26 metastatic liver tumor model in C26s.c.TB-mice. α-GalCer treatment resulted in complete rejection of metasatic Colon26 liver tumor in normal mice, but the antitumor effect of α-GalCer against metastatic liver tumor was significantly impaired in C26s.c.TB-mice. These results were consistent with the clinical data of α-GalCer treatment in

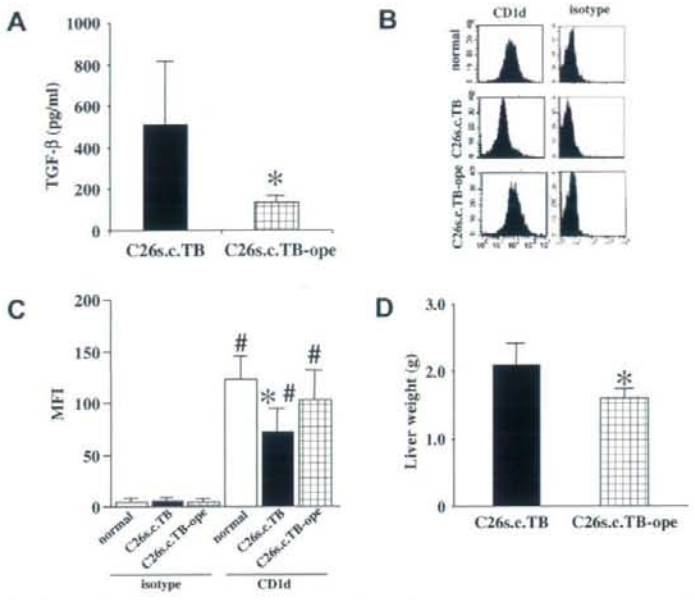

Fig. 6. Evaluation of serum TGF-β and CD1d expression on liver DCs and the antitumor effect of α-GalCer against metastatic liver tumor in surgical treated C26s.c.TB-mice. At 42 days, Colon26 subcutaneous tumors in C26s.c.TB-mice were surgically excised. Fourteen days later, liver DCs from surgically treated mice were prepared for comparison with liver DCs isolated from 42-day C26s.c.TB-mice. (A) Mice sera from C26s.c.TB-mice (C26s.c.TB) or surgically treated C26s.c.TB-mice (C26s.c.TB-ope) were harvested and were subjected to mouse TGF-β ELISA. Cytokine levels are reported in pg/ml (mean ± SD of triplicate samples). $^{*}p < 0.05$. (B, C) The expressions of CD1d on liver DCs from C26s.c.TB-mice (C26s.c.TB) or surgically treated C26s.c.TB-mice (C26s.c.TB-ope) were evaluated by flow cytometry. The representative flow cytometry data of CD1d expressions on liver DC were shown in Fig. 6B. The expression levels of CD1d molecules are reported as arbitrary MFI (mean ± SD of triplicate samples, Fig. 6C). $^{\#}p < 0.05$ vs. respective isotype control $^{*}p < 0.05$ vs. CD1d expression in normal mice. (D) C26s.c.TB-ope mice or C26s.c.TB-mice were injected into spleen with 5×10^5 Colon26 cells, and 24 h later α-GalCer was administered intraperitoneally ($N = 4$ in each group). Ten days after treatment, the livers were removed from treated mice and the liver weights of the groups were compared. $^{*}p < 0.05$. α-GalCer treated C26s.c.TB-ope mice vs α-GalCer treated C26s.c.TB-mice.

patients with advanced cancer, and encouraged us to investigate the detailed mechanism of the markedly reduced antitumor effect of α-GalCer in TB-mice to establish better α-GalCer treatment for cancer patients.

DCs have been implicated in the activation of NKT and NK cells in both mice and humans [1,6,12–17]. α-GalCer presented by CD1d molecules expressed on DCs activates NKT cells via recognition between CD1d molecules and Vα14–Jα281 invariant antigen receptor in mice [18]. Thus the expression of CD1d molecules on DCs is believed to be important for activation of NKT cells. Our study demonstrated that CD1d expressions on bone marrow-derived DCs were similar between normal and C26s.c.TB-mice, suggesting that the ability of differentiating DCs from precursor cells in bone marrow were same in both normal and C26s.c.TB-mice. In contrast, the CD1d expressions of liver DCs and spleen DCs in C26s.c.TB-mice were lower than those in normal mice. This is not unique to C26s.c.TB-mice, because decreased expression of CD1d molecules on liver DCs (not bone marrow-derived DCs) was also observed in CMS4 mouse sarcoma or BNL mouse hepatoma TB-mice (Tatsumi, unpublished data). These results suggested that some systemic immunosuppressive factors might modify the CD1d expression on DCs in TB-mice. Osman et al. demonstrated that α-GalCer administration resulted in activation of liver NKT cells with significant early disappearance of liver NKT cells in normal mice [19]. They also demonstrated that these phenomenon were not observed in CD1d(−/−) mice, suggesting that CD1d expressions play essential roles of liver NKT activation [19]. In our study, the early decreases of liver NKT cells were not observed after α-GalCer treatment in C26s.c.TB-mice. Based on these observations, the decreased expression of CD1d molecules on DCs might be associated with the impaired activation of liver innate immunity, thus resulting in an impaired antitumor effect of α-GalCer.

A normal mice liver contains lymphocytes that are usually enriched with NK and NKT cells; i.e., 25% NK cells and 30% NKT cells in contrast to peripheral blood that contains only 10% NK and 5% NKT cells

[20,21]. Efficient activation of abundant NKT cells and NK cells in the liver might be important in an antitumor effect against liver tumor. We and others have previously reported that sequential activation of both NKT cells and NK cells could be observed in the liver after α-GalCer administration. Although most NKT cells had disappeared from the liver within 12 h of α-GalCer administration [4,19], the antitumor effect against disseminated liver tumor depends on NK cells in the α-GalCer treatment, evidenced by that depletion of NK cells abolished the anti-metastatic tumor effect [4]. In the present study, we found the impairment of both the cytolytic activity of NK cells and an increase of the NK cell proportion in whole liver MNC in α-GalCer-treated C26s.c.TB-mice. These findings also offer the evidence that insufficient activation of liver NK cells might be associated with a poor antitumor effect of α-GalCer in TB-mice. The expressions of antigen-presenting related molecules, CD80 and CD86, on liver DCs in C26s.c.TB-mice were also lower than those in normal mice. Taken together, the presence of a tumor mass might modify the innate immune response in the liver and the maturation of liver DCs in TB-mice.

Several previous reports have demonstrated that TGF-β and IL-10 inhibit CD1d expression on DCs [10,11]. We hypothesize that the decreased expressions of CD1d might be associated with these immunosuppressive cytokines derived from the tumor mass. Our study demonstrated that Colon26 cells produce a large amount of TGF-β, but not IL-10, and that serum TGF-β level in C26s.c.TB-mice was significantly higher than that in normal mice, while the serum IL-10 level was not. Our results suggested that tumor-derived TGF-β might decrease CD1d expressions on liver DCs in C26s.c.TB-mice. Biswas et al. demonstrated that administration of anti-TGF-β neutralizing antibody inhibited metastatic cancer [22], suggesting that if the tumor-derived TGF-β had decreased in TB-mice, the liver immunological environment might be improved to develop antitumor immunity. Based on these results, we next examined serum TGF-β levels and the CD1d expression on liver DCs after surgical subcutaneous mass resection. Fourteen days after surgical resection, serum TGF-β in treated C26s.c.TB-mice had significantly decreased and the expressions of CD1d on liver DCs from treated C26s.c.TB-mice had significantly increased and recovered to the level of normal mice, suggesting that Colon26 tumor tissue derived TGF-β might modify the CD1d expression on liver DCs. More importantly, we demonstrated that the antitumor effect of α-GalCer against metastatic liver tumor was significantly improved in C26s.c.TB-ope mice. We believe that if complete resection of primary tumor could be achieved, the liver immune microenvironment might be expected to recover dramatically and cancer immunotherapy using α-GalCer might lead to better outcomes.

de Lalla et al. reported that the human invariant NKT cells are significantly enriched in chronically inflamed livers as compared with noninflamed ones although human liver harbors significantly less invariant NKT cells than the mouse one [23], suggesting that human invariant NKT cells might also play important roles in developing the chronic liver disease. Although the frequency of invariant Vα24 NKT cells is very low in humans, Vα24 NKT cells can be expanded by the stimulation of α-GalCer in cancer patients [7]. These suggested that the effector function of invariant NKT cells in human liver might be important for the establishing of new cancer treatments of α-GalCer.

The liver is the most common site of metastasis of gastrointestinal cancers (i.e., colorectal cancer, gastric cancer and pancreatic cancer). Thus, new therapeutic approaches of cancer immunotherapy for advanced liver tumor need to be developed. Our report is the first report demonstrating that the presence of a tumor mass might inhibit the activation of liver innate immune cells by α-GalCer due to decreased expression of CD1d on liver DCs. These findings indicate that α-GalCer treatment may represent a promising approach to preventing liver metastasis if the primary tumor can be completely controlled.

Acknowledgements

The authors thank Kirin Pharma Co. Ltd. (Gunma, Japan) for providing the α-galactosylceramide. This work was supported by a Grant-in-Aid from the Ministry of Education, Culture, Sports, Science and Technology of Japan, a Grant-in-Aid for Research on Hepatitis and BSE from the Ministry of Health, Labor and Welfare of Japan and Core Research for Evolutional Science and Technology (CREST) from Japan Science and Technology Agency.

References

[1] Kawano T, Cui J, Koezuka Y, Toura I, Kaneko Y, Sato H, et al. CD1d-restricted and TCR-mediated activation of Vα14NKT cells by glycosylceramides. Science 1997;278:1626–1629.

[2] Fujii S, Shimizu K, Kronenberg M, Steinman RM. Prolonged IFN-γ- producing NKT response induced with alpha-galactosylceramide-loaded DCs. Nat Immunol 2002;3:867–874.

[3] Gonzalez-Aseguinolaza G, de Oliveira C, Tomaska M, Hong S, Bruna-Romero O, Nakayama T, et al. α-Galactosylceramide-activated Vα 14 natural killer T cells mediate protection against murine malaria. Proc Natl Acad Sci USA 2000;97:8461–8466.

[4] Miyagi T, Takehara T, Tatsumi T, Kanto T, Suzuki T, Jinushi M, et al. CD1d-mediated stimulation of natural killer T cells selectively activates hepatic natural killer cells to eliminate experimentally disseminated hepatoma cells in murine liver. Int J Cancer 2003;106:81–89.

[5] Nakagawa R, Motoki K, Ueno H, Iijima R, Nakamura H, Kobayashi E, et al. Treatment of hepatic metastasis of the colon26

adenocacinoma with an α-galactosylceramide, KRN7000. Cancer Res 1998;58:1202–1207.
[6] Nieda M, Okai M, Tazbirkova A, Lin H, Yamaura A, Ide K, et al. Therapeutic activation of Vα24 + Vβ11 + NKT cells in human subjects results in highly coordinates secondary activation of acquired and innate immunity. Blood 2004;103:383–389.
[7] Giaccone G, Punt CJ, Ando Y, Ruijter R, Nishi N, Peters M, et al. A phase I study of the natural killer T-cell ligand α-galactosylceramide (KRN7000) in patients with solid tumors. Clin Cancer Res 2002;8:3702–3709.
[8] Tatsumi T, Takehara T, Yamaguchi S, Sasakawa A, Sakamori R, Ohkawa K, et al. Intrahepatic delivery of α-galatosylceramide pulsed dendritic cells suppresses liver tumor. Hepatology 2007;45:22–30.
[9] Takehara T, Uemura A, Tatsumi T, Suzuki T, Kimura R, Shiotani A, et al. Natural killer cell-mediated ablation of metastatic liver tumors by hydrodynamic injection of IFN alpha gene to mice. Int J Cancer 2007;120:1252–1260.
[10] Ronger-Savle S, Valladeau J, Claudy A, Schmitt D, Pequet-Navarro J, Dezutter-Dambuyant C, et al. TGFbeta inhibits CD1d expression on dendritic cells. J Invest Dermatol 2005;124:116–118.
[11] Gerlini G, Tun-Kyi A, Dudli C, Burg G, Pimpinelli N, Nestle FO. Metastatic melanoma secreted IL-10 down-regulates CD1 molecules on dendritic cells in metastatic tumor lesions. Am J Pathol 2004;165:1853–1863.
[12] Fernandez NC, Lozier A, Flament C, Ricciardi-Castagnoli P, Bellet D, Suter M, et al. Dendritic cells directly trigger NK cell functions: cross-talk relevant in innate anti-tumor immune responses in vivo. Nat Med 1999;5:405–411.
[13] Gerosa F, Baldani-Guerra B, Nisii C, Marchesini V, Carra G, Trinchieri G. Reciprocal activating interaction between natural killer cells and dendritic cells. J Exp Med 2002;195:327–333.
[14] Ferlazzo G, Tsang ML, Moretta L, Melioli G, Steinman RM, Munz C. Human dendritic cells activate resting NK cells and are recognized via the NKp30 receptor by activated NK cells. J Exp Med 2002;195:343–351.
[15] Kawano T, Cui J, Koezuka Y, Toura I, Kaneko Y, Sato H, et al. Natural killer-like nonspecific tumor cell lysis mediated by specific ligand-activated Vα14NKT cells. Proc Natl Acad Sci USA 1998;95:5690–5693.
[16] Kitamura H, Iwakabe K, Yahata T, Nishimura S, Ohta S, Ohmi Y, et al. The natural killer T (NKT) cell ligandα-galactosylceramide demonstrates its immunopoteniating effect by inducing interleukin (IL)-12 production by dendritic cells and IL-12 receptor expression on NKT cells. J Exp Med 1999;189:1121–1128.
[17] Ferlazzo G, Munz C. NK cell compartments and their activation by dendritic cells. J Immunol 2004;172:1333–1339.
[18] Seino K, Motohashi S, Fujisawa T, Nakayama T, Taniguchi M. Natural killer T cell-mediated antitumor immune responses and their clinical applications. Cancer Sci 2006;97:807–812.
[19] Osman Y, Kawamura T, Naito T, Takeda K, Van Kaer L, Okumura K, et al. Activation of hepatic NKT cells and subsequent liver injury following administration of α-galactosylceramide. Eur J Immunol 2000;30:1919–1928.
[20] Doherty DG, O'Farrelly C. Innate and adaptive lymphoid cells in human liver. Immunol Rev 2000;174:5–20.
[21] Mehal WZ, Azzaroli F, Crispe IN. Immunology of the healthy liver: old questions and new insights. Gatsroenterology 2001;120:250–260.
[22] Biswas S, Guix M, Rinehart C, Dugger TC, Chytil A, Moses HL, et al. Inhibition of TGF-beta with neutralizing antibodies prevents radiation-induced acceleration of metastatic cancer progression. J Clin Invest 2007;117:1305–1313.
[23] de Lalla C, Galli G, Aldrighhetti L, Romeo R, Mariani M, Monno A, et al. Production of profibrotic cytokines by invariant NKT cells characterizes cirrhosis progression in chronic viral hepatitis. J Immunol 2004;173:1417–1425.